

Research Paper

Multi-scale integrative analyses identify THBS2⁺ cancer-associated fibroblasts as a key orchestrator promoting aggressiveness in early-stage lung adenocarcinoma

Haitang Yang^{1*}, Beibei Sun^{2*}, Liwen Fan^{1*}, Wenyan Ma^{3*}, Ke Xu¹, Sean R. R. Hall⁴, Zhixin Wang¹, Ralph A. Schmid⁵, Ren-Wang Peng⁵, Thomas M. Marti⁵, Wen Gao⁶, Jianlin Xu⁷, Weiwei Yang⁸, Feng Yao¹

1. Department of Thoracic Surgery, Shanghai Chest Hospital, Shanghai Jiao Tong University; Shanghai, 200030, People's Republic of China.
2. Institute for Thoracic Oncology, Shanghai Chest Hospital, Shanghai Jiao Tong University; Shanghai, 200030, People's Republic of China.
3. Clinical Research Center, Shanghai Chest Hospital, Shanghai Jiao Tong University, Shanghai, 200030, People's Republic of China.
4. Wyss Institute for Biologically Inspired Engineering, Harvard University; United States.
5. Division of General Thoracic Surgery, Department of BioMedical Research (DBMR), Inselspital, Bern University Hospital, University of Bern; Bern, 3010, Switzerland.
6. Department of Thoracic Surgery, Huadong Hospital Affiliated to FuDan University, China.
7. Department of Respiratory Medicine, Shanghai Chest Hospital, Jiao Tong University; Shanghai, 200030, People's Republic of China.
8. School of Life Science, Hangzhou Institute for Advanced Study, University of Chinese Academy of Sciences, Hangzhou 310024, People's Republic of China.

*These authors contributed equally to this work.

 Corresponding authors: Feng Yao (yaofeng@shsmu.edu.cn), Department of Thoracic Surgery, Shanghai Chest Hospital, Shanghai Jiao Tong University; Shanghai, 200030, China. Tel. 021-222-00000; Fax. 021-222-00000; Weiwei Yang (wyang@sibcb.ac.cn), School of Life Science, Hangzhou Institute for Advanced Study, University of Chinese Academy of Sciences, Hangzhou 310024, China; Jianlin Xu (xujianlin1018@163.com), Department of Respiratory Medicine, Shanghai Chest Hospital, Jiao Tong University; Shanghai, 200030, China.

© The author(s). This is an open access article distributed under the terms of the Creative Commons Attribution License (<https://creativecommons.org/licenses/by/4.0/>). See <http://ivyspring.com/terms> for full terms and conditions.

Received: 2021.11.30; Accepted: 2022.03.20; Published: 2022.03.28

Abstract

Rationale: Subsets of patients with early-stage lung adenocarcinoma (LUAD) have a poor post-surgical course after curative surgery. However, biomarkers stratifying this high-risk subset and molecular underpinnings underlying the aggressive phenotype remain unclear.

Methods: We integrated bulk and single-cell transcriptomics, proteomics, secretome and spatial profiling of clinical early-stage LUAD samples to identify molecular underpinnings that promote the aggressive phenotype.

Results: We identified and validated THBS2, at multi-omic levels, as a tumor size-independent biomarker that robustly predicted post-surgical survival in multiple independent clinical cohorts of early-stage LUAD. Furthermore, scRNA-seq data revealed that THBS2 is exclusively derived from a specific cancer-associated fibroblast (CAF) subset that is distinct from CAFs defined by classical markers. Interestingly, our data demonstrated that THBS2 was preferentially secreted via exosomes in early-stage LUAD tumors with high aggressiveness, and its levels in the peripheral plasma associated with short recurrence-free survival. Further characterization showed that THBS2-high early-stage LUAD was characterized by suppressed antitumor immunity. Specifically, beyond tumor cells, THBS2+ CAFs mainly interact with B and CD8+ T lymphocytes as well as macrophages within tumor microenvironment of early-stage LUAD, and THBS2-high LUAD was associated with decreased immune cell infiltrates but increased immune exhaustion marker. Clinically, high THBS2 expression predicted poor response to immunotherapies and short post-treatment survival of patients. Finally, THBS2 recombinant protein suppressed *ex vivo* T cells proliferation and promoted *in vivo* LUAD tumor growth and distant micro-metastasis.

Conclusions: Our multi-level analyses uncovered tumor-specific THBS2+ CAFs as a key orchestrator promoting aggressiveness in early-stage LUAD.

Key words: early-stage lung adenocarcinoma, THBS2, exosome, cancer-associated fibroblast, immunotherapy

Introduction

Adenocarcinoma is the most common histological subtype of lung cancer. The lung cancer screening program greatly facilitates the early detection of lung adenocarcinoma (LUAD), leading to an improved prognosis over the years [1].

For early-stage LUAD patients without lymph node (N) metastasis (pathological [p] N0 stage), surgical resection can achieve a high curative rate, and adjuvant therapies are generally not recommended afterward. However, up to 20%~30% of these early-stage patients have a poor prognosis with a significantly compromised 5-year overall survival (OS) and recurrence-free survival (RFS) [2], defining a high-risk subset who may need additional adjuvant therapies after curative surgery.

In view of the presence of high-risk subsets, it is crucial to identify specific biomarkers that can stratify pN0-stage LUAD patients for subsequent precise management and facilitate the development of novel targeted strategies. To achieve this, extensive studies have been conducted to uncover potential classification models. Currently, a well-established and widely used model is the new IASLC (International Association for the Study of Lung Cancer)/ATS (the American Thoracic Society)/ERS (the European Respiratory Society) classification system [3], which displays significant prognostic and predictive values regarding tumor recurrence and death [4]. According to this model, early-stage LUADs predominant with mucinous, colloid, solid, or micropapillary components are characterized by dismal prognosis, thus defining a histological subtype-based model to identify high-risk subsets. Apart from that, previous studies also demonstrated other predictive clinicopathological biomarkers to determine the high-risk subsets [5, 6], e.g., tumor size, well-/moderately-/poorly differentiated histological status, visceral pleural involvement, lymphovascular invasion, despite the presence of heterogeneous conclusions [7]. However, the majority of these predictive models are histology- and phenotype-based only, but lack the underlying molecular underpinnings that drive this aggressive subtype. Given the absence of molecular characterization, it is still unknown about the optimal management for this high-risk subset, in that it remains controversial whether conventional adjuvant chemotherapy could generate benefits [8-11].

Besides, the above models are highly restricted to the availability of tumor tissue, which involves invasive procedures and difficulties to obtain serial samples. By contrast, liquid biopsy, e.g. cell-free DNA (cfDNA), circulating tumor cells (CTCs) and plasma exosomes, can overcome these disadvantages [12].

Among these, exosomes represent a more interesting liquid biomarker from the perspective of pathobiological roles in tumors [13]. An increasing number of studies have revealed that exosomes, which are ~40 to 100 nm vesicles secreted by a wide range of cell types, mediate the cross-talk among cells within or outside the tumor microenvironment (TME), promote cancer drug resistance and create a metastatic niche to facilitate tumor recurrence/metastasis [14].

Accumulating evidence has revealed the critical role of TME in promoting disease progression and treatment resistance [15]. The TME comprises various cell types, including stromal cells (predominantly cancer-associated fibroblasts (CAFs)), immune cells, and extracellular matrix (ECM) components. Among those, CAFs are the most abundant cell type in a variety of carcinomas, mediating the production of ECM components, such as collagens, glycosaminoglycans and glycoproteins, enhancing the invasive activity of cancer cells, and suppressing anti-tumor immunity [16]. Particularly, CAFs also represent one of the major sources secreting exosomes in cancer [17]. Nevertheless, the role of TME in the progression of early-stage LUAD is still unclear.

Here, by integrating multi-omic analyses of independent datasets, we provided the first evidence that THBS2, an exosome protein secreted by a specific subset of CAFs, serves as a robust biomarker for predicting OS and RFS as well as clinical treatment response in patients with pN0-stage LUAD. Functionally, CAFs-derived THBS2 promoted the aggressive phenotype by presumably modulating both cancer cells and tumor immunity, identifying THBS2+ CAFs as a candidate therapeutic target in early-stage LUAD.

Methods

Study design

The training dataset was based on The Cancer Genome Atlas (TCGA) LUAD cohort (**Figure 1**). Patients who had primary LUAD at pathologically confirmed pN0/M0-stage after radical surgery and reached the endpoints (cancer-related death or tumor recurrence) were included. Weighted gene co-expression analysis (WGCNA) was then performed by correlating the transcriptomic data (treatment-naïve) with clinical survival data (cancer-specific OS and RFS).

The most negatively correlated cluster (module) with RFS and OS was then selected to identify potential gene candidates whose high expression predicts poor prognosis of patients with early pN0-stage LUAD. Subsequently, the prognostic

capacity of the selected gene candidates was evaluated in the training cohort and independent external (at the transcriptomic and proteomic levels) and internal (at the protein level) cohorts. Finally, single-cell transcriptome and multiplexed

immunohistochemistry staining analyses, as well as *in vitro* and *in vivo* functional experiments were performed to decipher the major cellular subsets that contribute to the aggressive phenotype in pN0-stage LUAD (Figure 1).

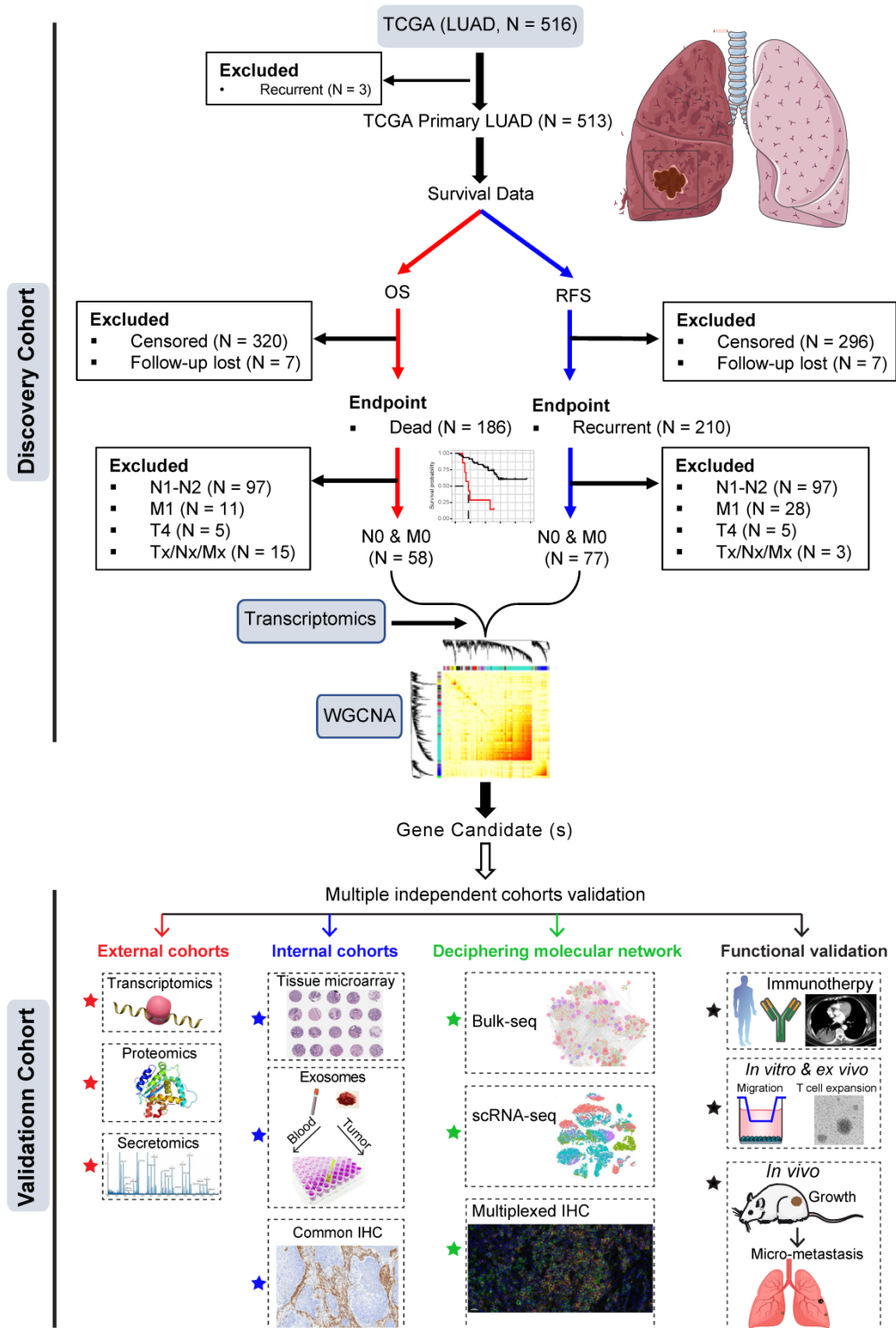


Figure 1. Study design. Early pN0-stage lung adenocarcinoma (LUAD) with complete survival endpoints (recurrence-free survival (RFS) and overall survival (OS) from The Cancer Genome Atlas (TCGA) database) was used as a training cohort. Following this, WGCNA (weighted gene co-expression analysis) analysis is used to identify molecular clusters that correlate with RFS and OS, which were then validated using multiple external and internal resected pN0-stage LUAD cohorts. Finally, the potential molecular networks and biological functions of the candidate molecules were deciphered with multi-dimensional evidence.

WGCNA and Function Enrichment Analyses

To identify the gene expression profiles associated with the protein levels of RFS and OS in pN0-stage LUAD, we applied the R package “WGCNA” to whole-genome transcriptomic data. In WGCNA, genes were clustered according to their co-expression patterns [18-20], with which a gene co-expression network was then constructed. Genes were grouped into different modules (clusters) using the dynamic tree cut algorithm, according to topological overlap matrix (TOM)-based dissimilarity. The module eigengene (ME) was calculated based on the first principal component of each module. The ME values were correlated (Pearson) with sample traits (RFS and OS). Here, we set the soft-thresholding power at 12 (scale-free R2 was approximately 0.9), cut height at 0.25, and minimal module size to 30 to identify key modules. The module significantly correlated with sample traits was selected to explore its biological functions, such as Gene Ontology (GO), Kyoto Encyclopedia of Genes and Genomes (KEGG) and Reactome pathway enrichment analyses, using the R package “clusterProfiler” [21, 22]. Hub genes were defined as the top 30 intramodular connected genes.

Patient samples (tissue and blood)

The treatment-naïve samples of lung cancer patients for the present study were all taken from hospitalized patients in the Department of Thoracic Surgery at Shanghai Chest Hospital.

Peripheral blood samples were collected from treatment-naïve LUAD patients and healthy donors. Samples were centrifuged at 4 °C for 10 min at 1000 g to separate plasma from blood cells. Supernatants were collected, divided into aliquots and stored at -80 °C until use.

This study was approved by the institutional review board (#KS(Y)21316). All patients had signed informed consent for inclusion of their clinical data and specimens in our Lung Biobank and use in research projects, according to the recommendation of the ethical committee of Shanghai Chest Hospital.

Follow-up

RFS was defined as the interval between surgery and recurrence; if recurrence was not diagnosed, the date of death or last follow-up was recorded. OS was defined as the interval between surgery and death.

Immunotherapy response assessments

After completion of two cycles of immunotherapy, positron emission tomography/computed tomography (PET/CT) or CT scans were performed to evaluate the therapeutic response. The

response was assessed based on the Response Evaluation Criteria in Solid Tumors (RECIST) (version 1.1) [23].

Preparation of single-cell suspensions from surgically resected samples

Sample preparation

Two paired (primary lung tumor [pT1N0M0] and matched normal lung tissue) lung samples were collected and immediately transferred for single-cell isolation. Tumor tissues and tumor-adjacent normal lung tissues were obtained during surgery at Huadong Hospital (Shanghai, China). Tumor samples were collected from three different sites of the tumor bed. Normal lung tissue was separated from the malignant region by at least 5 cm. The tissues were rinsed with cold PBS (Cytiva, SH30256.01) to wash out the blood and dead cells. Then, they were put in 1.5 mL cooled tissue storage solution (Miltenyi, 130-100-008) and transferred to the laboratory on ice. The tissues were minced into small pieces (smaller than 1 mm³) within 5 min, subjected to digestion buffer (4.7 mL DMEM (Cytiva, SH30243.01) + 325 µL enzyme mix (Miltenyi, 130-095-929)) and incubated at 37 °C for 30 min on a shaker. The samples were passed through a 70 µm filter (Miltenyi, 130-095-823) and centrifuged at 300 g at 4 °C for 7 min. The remaining blood cells and the dead cells were removed using red blood cell lysis solution (Miltenyi, 130-094-183) and Ficoll-Paque PLUS (Cytiva, 17144002-1) separation. The cell pellets were finally resuspended in DMEM + 10% FBS (Thermo Fisher Scientific, 10099141C) before microscopic inspection and scRNA-seq library construction.

Single-cell RNA library construction, sequencing and data processing

Single-cell suspensions (1 × 10⁶/mL), of which the viability was higher than 80%, were submitted to 10X genomics Chromium Controller to generate single-cell gel beads in emulsion (GEMs). The library was constructed by Chromium Next GEM Chip G Single Cell Kit, Single Cell 3' GEM, Library & Gel Bead Kit v3.1, Library Construction Kit v3.1, and i7 Multiplex Kit (10X genomics) following the manufacturer's instruction. Briefly, the captured cells were lysed, and the released RNA was barcoded via reverse transcription in individual GEMs. Reverse transcription was performed at 53 °C for 45 min, followed by 85 °C for 5 min, after which the temperature was held at 4 °C. Complementary DNA amplification and quantification were performed to build the 3' gene libraries, whose quality was assessed by a 2100 Bioanalyzer (Agilent). Then, libraries were sequenced by Illumina Nova-seq 6000 with a

paired-end 150-base pair (PE150) reading strategy.

scRNA-seq data processing

Raw gene expression matrix was generated for each sample using the 10X genomics Cell Ranger toolkit (version 4.0.0) and mapped to the GRCh38 human reference genome. After that, the output was analyzed by R software (version 3.6.3) with the Seurat package (version 3.2.0) for quality control and downstream analysis [24]. In brief, genes expressed at a proportion >0.1% of the data were selected for further analyses. Low-quality cells were removed if they met the following criteria: (1) < 500 unique molecular identifiers (UMIs), (2) < 200 or > 10000 genes, (3) > 10% unique molecular identifiers (UMIs) derived from the mitochondrial genome, (4) > 10% UMIs derived from the red-cell genome, or (5) predicted doublets by the Scrublet package (version 3.7.3) [25].

scRNA-seq data normalization, dimensional reduction, and clustering

After the removal of low-quality cells, the datasets collected from different samples were integrated using FindIntegrationAnchors and FindIntegrateData function with default parameters to remove the batch effect [26]. The gene expression matrix was normalized by the NormalizeData function, and 2000 features with high cell-to-cell variation were calculated using the FindVariableFeatures function. To reduce the dimensionality of the datasets, the RunPCA function was conducted with default parameters on scaled data generated by the ScaleData function. During this process, we implemented Clustree algorithm (“clustree” R package; <https://cran.r-project.org/web/packages/clustree/vignettes/clustree.html>) to increase gene representation and achieve optimal cluster separation [27]. Next, the ElbowPlot, DimHeatmap, and JackStrawPlot functions were used to identify the true dimensionality of each dataset, as recommended by the Seurat developers. Last, the first 20 principal components were applied to clustering by FindNeighbors and FindClusters functions, and RunTSNE function was performed with default settings for nonlinear dimensional reduction. For all 43,779 cells, the clustering results were visualized with the UMAP (Uniform Manifold Approximation and Projection) scatter plot.

Cell type annotation and cluster marker identification

The annotations of cell identity on each cluster were defined by the expression of known marker genes, which were identified using the FindAllMarkers function provided by Seurat. The fibroblasts were identified according to the known

markers: *DCN*, *LUM*, *COL1A1*, *COL1A2*. Clusters were also confirmed by identifying significantly highly expressed marker genes in each cluster and then comparing them with the known cell-type-specific marker genes. By implementing the Clustree algorithm (“clustree” R package), the 332 CAFs were further categorized into 10 clusters.

Gene set enrichment analysis

We conducted the gene set enrichment analysis (GSEA) for differentially expressed genes between THBS2+ (positive) and THBS2- (negative) cancer-associated fibroblasts using clusterProfiler (version 4.0.5) and GSEABase (version 1.54.0) R toolkit with default settings [28]. Gene set used was hallmark gene set from the Molecular Signatures Database (MSigDB) [29].

Cell-cell interaction network in lung cancer samples

Cell-cell interaction network was determined by the CellChat R toolkit (version 1.1.2, <https://github.com/sqjin/CellChat>), an intercellular interaction analysis tool that studies ligand-receptor action in specific signaling pathways [30]. To explore the intercellular interaction in the tumor micro environment, gene expression matrices and metadata with major cell annotations from cancer samples were used as input for the CellChat software. Briefly, the cell-cell interaction was measured by quantification of ligand-receptor pairs among different cell types.

Transwell assay

The migration assay was performed using Transwell plates (24-well chamber with 8.0 μm pore size; Corning, NY, USA). Cells were starved overnight in media containing only 1% FBS. Briefly, 10^5 LUAD cells (incubated with PBS or 50 ng/mL THBS2 recombinant protein) were resuspended in the upper compartment (containing 200 μL FBS-free medium), with the lower compartment supplied with 10% FBS-containing media (800 μL). All of the results were obtained from three independent experiments.

Exosome isolation, purification and characterization

LUAD (pN0M0; N = 5) and normal adjacent tissue (NAT; N = 5), as well as blood plasma samples (2 mL; pN0M0-LUAD, N = 5; healthy controls, N = 5), were obtained freshly from Shanghai Chest Hospital. Combination of size-exclusion chromatography (SEC) (Echo9101A-30 mL, Exosupur kit, Echobiotech) and ultracentrifugation was used to purify exosomes in plasma [31] and tissue [32, 33].

For isolating exosomes from blood plasma, fresh peripheral blood samples from individuals were collected in EDTA tubes following a regular

venipuncture procedure. After centrifugation at $3,000 \times g$ for 15 min at 4°C , the plasma was aspirated and stored at -80°C before use. Samples were filtered through a $0.22 \mu\text{m}$ filter and added to the SEC column, 2 mL collected plasma fractions were centrifuged at $150,000 \times g$, 4°C for 4 h to further pellet the exosomes [31]. The pellet was resuspended in PBS and centrifuged again $150,000 \times g$, 4°C for 2 h. Finally, the supernatant was removed and resuspended in $100 \mu\text{L}$ PBS. The quantities of isolated exosomes were determined using a BCA Protein Assay Kit (Beyotime, Shanghai, China). Concerning the comparison of exosomal THBS2 levels in the plasma of LUAD patients, we used the same volume (2 ml) of plasma (stored at -80°C within 1 year).

For isolating exosomes from lung tissue, human pN0M0-stage LUAD and the normal adjacent lung tissues were gently dissociated into small pieces ($\sim 2 \times 2 \times 2 \text{ mm}$) and frozen at -80°C . Exosomes were separated from tissue using the protocol established previously by Vella, et al. [32], with minor modifications. The dissociation mixture was based on the Miltenyi Human Tumor Dissociation Kit (Miltenyi Biotec, cat. no. 130-095-929). Before starting, enzymes H, R and A were resuspended according to the manufacturer's instructions. Dissociation mix containing 2.2 mL RPMI, $100 \mu\text{L}$ enzyme H, $50 \mu\text{L}$ enzyme R and $12.5 \mu\text{L}$ enzyme A was prepared immediately before use. A small ($\sim 200 \text{ mg}$) piece of tissue was weighed and briefly sliced on dry ice and then incubated in the dissociation mixture for 10-15 min at 37°C . The dissociated tissue was filtered through a $70 \mu\text{m}$ filter gently twice to remove residual tissues. Then the suspension was spun at $300 \times g$ for 10 min at 4°C , and the supernatant was transferred to a fresh tube and spun at $2000 \times g$ for 10 min at 4°C . Cell-free supernatant was spun at $10,000 \times g$ for 20 min at 4°C and filtered through a $0.22 \mu\text{m}$ filter gently and slowly for further depletion of cell debris. The collected suspension was then processed by ultracentrifugation (UC) at $150,000 \times g$ for 2 h at 4°C . The pellet was resuspended in 1 mL phosphate-buffered saline (PBS) and further purified using Exosupur® columns (Echobiotech, China). Fractions were concentrated to $200 \mu\text{L}$ by 100 kDa molecular weight cut-off Amicon® Ultra spin filters (Merck, Germany). Regarding the comparison of exosomal THBS2 levels in the LUAD tumor tissue, we used the same weight (0.5 g) of frozen (-80°C) tumor tissue (removing the adjacent normal tissue).

The morphology of purified exosomes was identified by transmission electron microscopy (H-7650, Hitachi Ltd., Tokyo, Japan); briefly, $10 \mu\text{L}$ exosomes solution was placed on a copper mesh and incubated at room temperature for 1 min. After

washing with sterile distilled water, the exosome was contrasted by uranyl acetate solution for 1 min. The sample was then dried for 2 min under incandescent light. The copper mesh was observed and photographed under a transmission electron microscope. The size and purity of exosomes were measured by Nanoparticle Tracking Analysis (NTA) using ZetaView PMX 110 Nanoparticle Analyzer (Particle Metrix, Meerbusch, Germany); the identity of exosomes was validated using three positive exosomal markers (CD9, TSG101 and HSP70) and one negative marker (Calnexin) by western blot.

Exosome protein quality and enzyme-linked immunosorbent assay (ELISA)

Total Protein Extraction

The exosome samples isolated and purified at the same conditions were lysed with lysis buffer containing 100 mM NH_4HCO_3 , 6 M Urea and 0.2% SDS, followed by ultrasonication on ice. The lysate was centrifuged at $12,000 \text{ g}$ for 15 min at 4°C and the supernatant was collected. Each sample was reduced with 10 mM DTT for 1 h at 56°C and alkylated with iodoacetamide for 1 h at room temperature in the dark. Then samples were mixed with 4 times volume of acetone and incubated at -20°C for 2 h. After centrifugation, the precipitation was collected and washed by cold acetone. The pellet was dissolved by 0.1 M TEAB and 6 M Urea.

Protein Quality Test

The protein quality of samples was calculated by the BSA standard protein solutions curve with Pierce™ BCA Protein Assay Kit (Product No. 23,225, Thermo Scientific, USA). $10 \mu\text{L}$ standard samples were pipetted into 96-well plates, then added $200 \mu\text{L}$ BCA kit to each well. Then the plate was covered and incubated at 37°C for 30 min. The absorbance was set at 562 nm on the plate reader, and the standard curve was used to measure the protein concentrations of each isolated sample. Each sample solution with different dilution multiples was repeated three times.

$20 \mu\text{L}$ protein sample was loaded to 12% SDS-PAGE gel electrophoresis. The concentrated gel was performed at 80 V for 20 min, and the separation gel was performed at 120 V for 90 min. The gel was stained by coomassie brilliant blue R-250 and decolorized until the bands were visualized clearly. assessed using a microplate reader (Bio-Rad Laboratories, Hercules, CA, USA).

Proteinase K Assay

To determine the location (membrane or inside of exosomes) of exosomal THBS2 protein, proteinase K assay was performed, as described previously [34].

20 mL plasma of 6 LUAD patients were used to purify exosomes (500 μ L; concentration: 1062 ng/ μ L), and were incubated in (1) PBS (control), (2) 1.2 μ g/mL Proteinase K (Promega, Catalog Number: V3021; in PBS) alone, (3) 0.5% Triton X-100, or (4) combined Proteinase K and Triton X-100. The samples were then subjected to immunoblot to test TSG-101 (exosomal intra-membrane protein; as positive control), CD9 (exosomal trans-membrane protein; as positive control), THBS2.

Common IHC, multiplexed IHC, tissue microarray (TMA) and quantitative analysis

Immunohistochemistry (IHC) was performed on 6- μ m thick sections as previously described [35]. Antibodies for common or multiplexed IHC were listed in **Table S1**.

For multiplexed IHC, three groups were set. 1) multiplexed IHC of THBS2, FAP, S100A4 and α SMA was performed according to the manufacturer's instructions (Absin, 5-Color Multiple IHC Kit; #abs50013); 2) multiplexed IHC of THBS2, CD19, CD8, FOXP3, CD68 and CD56 were performed according to the manufacturer's instructions (Absin, 7-Color Multiple IHC Kit; #abs50015); 3) multiplexed IHC of CD4, CD8, CD19 and PD-1 was performed according to manufacturer's instruction (Absin, 5-Color Multiple IHC Kit; #abs50013), as previously described [36]. Briefly, slide sections of formalin-fixed paraffin-embedded (FFPE) block were deparaffinized in xylene and rehydrated in ethanol. After microwave antigen retrieval in heated citric acid buffer (pH 6.0) for 10 mins, endogenous peroxidase activity was blocked by 3% H₂O₂ for 10 mins, and nonspecific binding sites were blocked by goat serum for 10 mins. Primary antibodies were incubated for 1 h in a humidified chamber at room temperature, followed by incubation with the corresponding secondary horseradish peroxidase-conjugated polymer. Visualization of each target was accomplished using fluorescein TSA Plus (1:100). Then, the slide was again placed in a heated citric acid buffer (pH 6.0) using microwave antigen retrieval to remove redundant antibodies before the next step. Finally, nuclei were subsequently visualized with DAPI (Absin Bioscience Inc., 5 μ g/mL), and the sections were coverslipped using antifade mounting medium (Absin 1:50).

For TMA construction, we retrospectively analyzed data from 93 patients who underwent surgery for lung cancer between 2004 and 2009 at the Department of Thoracic Surgery, Shanghai Chest Hospital. TMA slides were constructed as previously described in a protocol by Fedor HL et al. [37].

Image acquisition and data quantification

For common IHC and TMA sections, whole slide images were acquired using Grundium Ocus[®] microscope scanners. The THBS2 staining intensities of cancer and stromal cells in the images of full tissue sections were automatically analyzed and quantified using QuPath open-source software (version 0.2.4), where the DAB channel intensity of THBS2 (membrane and cytoplasm OD value) was extracted for each section [38]. For the classification of cancer cells, stromal cells, and necroptosis, multiple training regions representing typical morphologies of cancer and stromal cells as well as necroptotic regions are annotated first. Based on this, the unique parameters of each cell type were generated, which were then applied to the whole slide images.

For multiplexed IHC, slides were scanned and imaged using the Panoramic MIDI[®] platform and were analyzed in batches using HALO[®] and R scripts for the quantification of positively stained cells as previously described [36]. Consequently, we were able to quantify the positively-stained cells with one or combination markers. With this, we know how many cells are positive for single (e.g. THBS2+ only), double (e.g. THBS2+S100A4+), or triple (e.g. THBS2+S100A4+FAP+), quadruple (e.g. THBS2+S100A4+FAP+ α SMA+) staining.

Public Data acquisition and bioinformatic analysis

LUAD patient datasets

Transcriptomic and proteomic profiles as well as clinical parameters of primary LUAD patients from multiple public cohorts, including 9 microarray datasets (GSE10072 [39]; GSE32863 [40]; GSE63459 [41]; GSE68571 [42]; GSE72094 [43]; GSE30219 [44]; GSE29013 [45]; GSE14814 [46]; GSE121841 [47]) from GEO (Gene Expression Omnibus; <https://www.ncbi.nlm.nih.gov/geo/>), 1 RNA-sequencing dataset from a high-quality East Asian LUAD cohort [48], 3 transcriptomic and proteomic profiles from three recent publications in Cell [49-51], and 1 RNA-Seq dataset from TCGA, as well as a dataset from the KM plotter portal (<https://kmplot.com/analysis/>) [52]. Only patients who met the following three criteria were included: i) detailed TNM (8th) staging information containing stage I, IA, IB or T1-3N0M0 [53]; ii) overall survival information incorporating follow-up time and vital status; and iii) appropriate sample size. Of note, of the 5 datasets (GSE10072; GSE30219; GSE32863; GSE63459; GSE68571), there were only transcriptomic data of early-stage LUAD and matched normal lung but without the survival data in GSE10072 and GSE32863. Although the

survival data in GSE63459 were available, the cancer-related death only occurred in 5 patients in the entire cohort, leading to the fact that there are no sufficient endpoint events for analysis. For GSE68571, the survival data were provided, but our analysis (not shown) suggested a dramatical survival difference between the THBS2-high vs. THBS2-low pN0-stage LUAD, although the significance was not reached, which is largely due to the short follow-up in this study cohort and thus the median survival in the two subgroups was not reached. In addition, concerning the proteomic profiles from three recent publications in Cell [49-51], only one [51] but not the other two datasets [49, 50] provided the survival data. However, in the former dataset [51], there was no data of the matched normal lung tissue available. As such, we were only able to show the association between THBS2 protein level and survival with the former dataset, whereas comparing the difference in the THBS2 protein level between the pN0-stage LUAD and matched normal lung tissue with the latter two datasets. The clinical information could be found in Supplementary Table 1 of each publication. Raw CEL files, the corresponding chip platform and metadata were downloaded and normalized. The R packages “limma” and “edgeR” were used to normalize the data and identify the differential gene or protein expression, respectively [35].

Reverse phase protein array (RPPA) dataset

The level 4 RPPA data (normalized and batch effects removed) of LUAD patients were obtained from The Cancer Proteome Atlas (TCPA) [54]. Normalization of RPPA data was processed as follows: 1) calculate the median of each protein across all samples; 2) subtract the median (from step 1) from values of each protein in all samples; 3) calculate the median of all proteins in each sample; 4) subtract the median (from step 3) from values of each sample. The detailed information could be found at the TCPA portal: tcportal.org/tcpa/faq.html.

Immunotherapy datasets

Datasets with immunotherapy response data were downloaded and reanalyzed through GSE135222 (human lung cancer [55]), GSE78220 (human melanoma [56]), and GSE63557 (mouse mesothelioma [57]).

Gene signatures

Immune subtype models

C1-6 immune subtype models were generated according to a previously curated dataset [58]. Briefly, C1 (wound healing) subtype had elevated expression of angiogenic genes and a high proliferation rate; C2

(IFN-g dominant) subtype had the highest M1/M2 macrophage polarization, a strong CD8 signal and, together with C6, the greatest TCR diversity, and also showed a high proliferation rate; C3 (inflammatory) subtype was characterized by elevated Th17 and Th1 genes and low to moderate tumor cell proliferation; C4 (lymphocyte depleted) subtype displayed a more prominent macrophage signature, with Th1 suppressed and a high M2 response; C5 (immunologically quiet) subtype exhibited the lowest lymphocyte and highest macrophage responses, dominated by M2 macrophages. The C6 (TGF- β dominant) subtype displayed the highest TGF- β signature and a high lymphocytic infiltrate with an even distribution of the type I and type II T cells.

TME subtype models

TME subtype models were established by integrating multiple immunotherapy-associated dataset collections. The curated annotation and transcriptomic data of different cohorts were downloaded directly from the supplementary files of the corresponding publication [59].

Immune infiltrates estimation

QuantIseq, an algorithm that was specifically developed for RNA-sequencing data, was used to [60] estimate immune cell infiltrates. Briefly, normalized expression data (as transcripts per millions (TPM)) of pN0-stage LUAD tumors of TCGA cohort were used as inputs and then quantified via deconvolution the proportions of six different immune cell types (CD8+ T cells, non-regulatory CD4+ T cells, B cells, M1 macrophages, M2 macrophages natural killer [NK] cells) using the “quantiseqr” package in R.

Tumor purity evaluation

We implemented the ABSOLUTE-algorithm-based estimation of tumor purity, which could be directly downloaded from the UCSC portal (<https://xenabrowser.net/datapages/>, TCGA LUAD dataset).

T cell proliferation

T cell proliferation and activation assay were described previously [61, 62]. Briefly, peripheral blood mononuclear cells (PBMCs) were isolated from patient donors using Ficoll-Paque™ Plus (GE Healthcare Life Sciences) density gradient centrifugation. Then, purified CD3+ T cells were isolated from the PBMCs using the EasySep™ Human T Cell Isolation Kit (StemCell Technologies; catalog No. #17751) according to the manufacturer’s instructions. Single cells were expanded using an expansion media (Immunocult, StemCell Technologies; catalog No. #10981) consisting of 10 ng/mL of recombinant

human IL-2 (StemCell Technologies; catalog #78036.1) and anti-CD3/CD28 beads (StemCell Technologies; catalog No. #10971). Cells were grown in tissue culture-treated 12-well plates, fresh media changes were made every 3–4 days until cell colonies were evident. Then the same number of PBMCs were cultured in the expansion media containing 0, 100, 200 or 500 ng/mL THBS2, respectively, for 96h.

Animal experiments

Female BALB/c nude and C57BL/6 mice (6 weeks old) purchased from JSJ-lab (Shanghai, China) were used for animal experiments with the human LUAD cell line (A549) and mouse LUAD cell line (Lewis LLc cells), respectively. For A549 or LLc xenografts, tumor cells 1:1 mixed with Matrigel (356231; Corning) were subcutaneously inoculated in the left and right flanks (10^5 cells/injection). Mice were divided into 2 groups: 1) PBS group (N = 7) and 2) THBS2 (50 μ g/mL, human recombinant THBS2, Catalog #1635-T2-050, Bio-Techne China Co. Ltd.; mouse recombinant THBS2, Catalog #ABIN3011848, Atlas antibodies, Germany) group (N = 5). Tumor size/volume was calculated by the formula: $(D \times d^2)/2$, where “D” refers to the long tumor diameter and “d” the short tumor diameter [35, 63].

Statistical analyses

Data are presented as the mean \pm s.d., with the indicated sample size (n) representing biological replicates. Comparisons between two groups were carried out using parametric Student’s two-tailed unpaired t-test for normally distributed data. If data were not distributed normally, a nonparametric Wilcoxon rank-sum test (for unpaired) was used between the two groups. Comparisons among three groups were determined by one-way/two-way analysis of variance (ANOVA) and Bonferroni’s multiple comparison test. Statistical significance was determined by using GraphPad Prism 8 or R software (version 4.0.3, <http://www.r-project.org>). Survival analysis was performed using the “survminer” and “survival” R packages. Tumor samples within all datasets were divided into two groups based on the best-separation cut-off value of THBS2 (mRNA or protein level) to plot the Kaplan–Meier survival curves and perform multivariate Cox regression (forest plot) analysis to evaluate the risk significance of each variable for RFS and OS. $p < 0.05$ was considered statistically significant.

Results

Gene clusters correlated with survival of patients with pN0-stage LUAD

Our discovery cohort revealed several gene

modules that were significantly correlated with RFS (Figure S1A; Figure 2A) and OS (Figure S1B; Figure 2B) in pN0-stage LUAD. Genes in the positively correlated modules indicate that their abundance (co-expression) correlates with longer survival, while the negatively correlated modules signify that their abundance (co-expression) correlates with shorter survival. Notably, the correlation of these gene clusters with RFS and OS was independent of the pathological T (tumor size) stage (Figure 2A, 2B).

We then focused on the negatively correlated black (corresponding to RFS, p -value = 0.03) and pink (corresponding to OS, p -value = 8×10^{-4}) modules, given that their high expression predicts poorer prognosis (Figure 2A, 2B), thus making them better biomarker candidates concerning clinical applications. GO biological functional analysis revealed that genes in the black (N = 168) and pink (N = 259) modules were mainly enriched for ECM/stromal signature (Figure 2C, 2D; Figure S2A, 2B).

Of note, there was a high overlap (27 out of 30) of the top 30 most connected genes between the black and pink modules (Figure 2E), thereby identifying the genes whose high expression was consistently related to tumor relapse and poor survival of patients with pN0-stage LUAD. Since the association of the ECM/stromal gene signature with prognosis could be due to the difference in stromal abundance between tumors from patients with poor and good prognosis, we then compared the tumor purity from the two groups (poor vs. good prognosis), and found out that there was no difference (Figure 2F). Collectively, we identified a set of genes whose expression correlated with post-surgical survival in patients with pN0-stage LUAD.

Discovery of candidate biomarker protein THBS2

Among the top10 best-connected genes correlating with poor prognosis (both OS and RFS) (Figure 2E), integral membrane glycoprotein THBS2 (thrombospondin 2) was particularly interesting for the following reasons: 1) it is the top connected genes within RFS/OS (first/second-ranked); 2) it is a secreted glycoprotein that mediates cell-cell and cell-matrix interactions and plays a potentially critical role in cancer cell-stroma communications (Figure S3A); 3) like many other glycoproteins that have been routinely used as cancer diagnostic biomarkers in clinic, e.g. carcinoembryonic antigen and carbohydrate antigen 125, THBS2 can also be secreted by LUAD tumors (Figure S3B), and detected in peripheral blood of patients [64–66], highlighting its promises as a liquid biopsy marker for early-detection or tumor recurrence surveillance of lung cancer; 4)

More importantly, compared with THBS2 alone, combining the top 5 genes (*THBS2*, *COL3A1*, *COL5A2*, *COL1A2* and *COL5A1*) did not significantly improve the predictive ability for RFS and OS (**Figure 2G**), which is due to the highly mutual positive correlation among these genes (**Figure S3C**). This analysis highlights the rationale for using a single marker THBS2 instead of a combined gene-signature as a predictive biomarker; 5) Previous evidence has revealed THBS2 as a prognostic biomarker (either good or poor) in several cancer types [67-69]; 6) However, little is known about its role in promoting the aggressiveness of early-stage LUAD. Together, these characteristics make THBS2 a highly interesting candidate from the perspectives of cancer detection and prognostic biomarkers, as well as a potential therapeutic target [70].

In the TCGA training cohort, separate univariate and multivariate Cox survival analyses confirmed that high expression of *THBS2* was associated with poor OS (**Figure S3D**) and RFS (**Figure S3E**) in pN0-stage LUAD. Additionally, we investigated the factors that potentially influence the expression of THBS2 in early-stage LUAD, and intriguingly, we identified that smoking history was significantly associated with THBS2 expression (**Table S2**), which requires further investigations. Moreover, compared to normal lung tissues, pN0-stage LUAD had a higher expression of *THBS2*, which was much higher in the recurrent LUAD samples (**Figure S3F**). Collectively, the above data suggest THBS2 as a potentially desired biomarker predicting the poor prognosis in pN0-stage LUAD.

Cross-validation of THBS2 in multiple independent datasets

To evaluate the reliability of our findings, multiple independent, external and internal datasets were then included. Overall, clinical pN0-stage LUAD tumor samples had significantly higher expression of *THBS2* across all datasets compared to the matched normal lung tissue, despite the presence of its heterogeneous distribution among individual primary lung tumors (**Figure S4A**).

Mining multiple datasets revealed that high expression of *THBS2* was linked with poor OS and RFS in pN0-stage LUAD patients (**Figure S4B-D**). Recent real-world evidence supports the management of adjuvant chemotherapy in high-risk early-stage LUAD patients, despite the presence of heterogeneous conclusions [8-11]. More recently, adjuvant epidermal growth factor receptor (EGFR) tyrosine kinase inhibitors (TKIs) were also recommended in IB-IIIa stage LUAD after surgery [71]. In a recent resource dataset [48], we were able to

evaluate the association between *THBS2* and the survival of pN0-stage LUAD patients treated with adjuvant chemotherapy or EGFR-TKIs after surgery. Interestingly, we observed that in pN0-stage I LUAD patients treated with chemotherapy or EGFR-TKIs, high expression of *THBS2* was also significantly associated with poor OS (**Figure S4B**), suggesting that THBS2 might mediate resistance to chemotherapy or EGFR-TKIs in LUAD patients. In agreement, analysis of an independent public RNA-seq dataset obtained from biopsies of EGFR-mutant LUAD treated with osimertinib (a third-generation of EGFR-TKIs) further confirmed that *THBS2* gene expression significantly increased in the post-osimertinib (resistance) biopsies (**Figure S4E**) [72]. Previous evidence showed the failure of chemotherapy to provide additional survival benefits for patients with pN0-stage IB lung cancer after surgery [8], which was likely due to the absence of stratification biomarkers.

Given that the high mRNA level of *THBS2* is predictive of prognosis, we next sought to determine whether there is a correlation between the mRNA and protein levels of THBS2 in LUAD samples. Based on two recent high-quality multi-omics datasets that represent Western and Asian LUAD populations [49, 50], we observed that there was a high consistency between the mRNA and protein levels of THBS2 in both Western and Asian LUAD cohorts (**Figure 3A**). Interestingly, this correlation does not exist in the matched normal lung tissue (**Figure 3B**), suggesting a LUAD-specific pattern. Along the same lines, at the protein level, pN0-stage I LUAD had significantly higher THBS2 protein expression than matched normal lung tissue (**Figure 3C**). Importantly, the high THBS2 protein level was linked with short OS and RFS in pN0-stage LUAD (**Figure 3D**) and poor differentiation status (marking a more aggressive state) of early pN0-stage LUAD samples (**Figure 3E**).

Furthermore, as an internal validation, we randomly selected (from a prospectively established lung tumor biobank by a pathologist) pN0-stage LUAD patients who survived less ($N = 5$) or more ($N = 5$) than 5 years, demonstrating that THBS2 protein expression was significantly higher in pN0-stage I LUAD patients with shorter OS than in those with longer OS ($p=0.0024$) (**Figure 3F**). Finally, in an independent, prospectively-established, internal LUAD cohort (tissue microarray data; $N = 93$), the THBS2 protein level was identified as an independent influencing factor of OS (**Figure S5A, B; Table S3**). Notably, in line with the public datasets (**Figure 3; Figure S4**), the THBS2 protein level is significantly higher in the tumors, compared to the matched normal lung tissue (**Figure S5A; Table S3**).

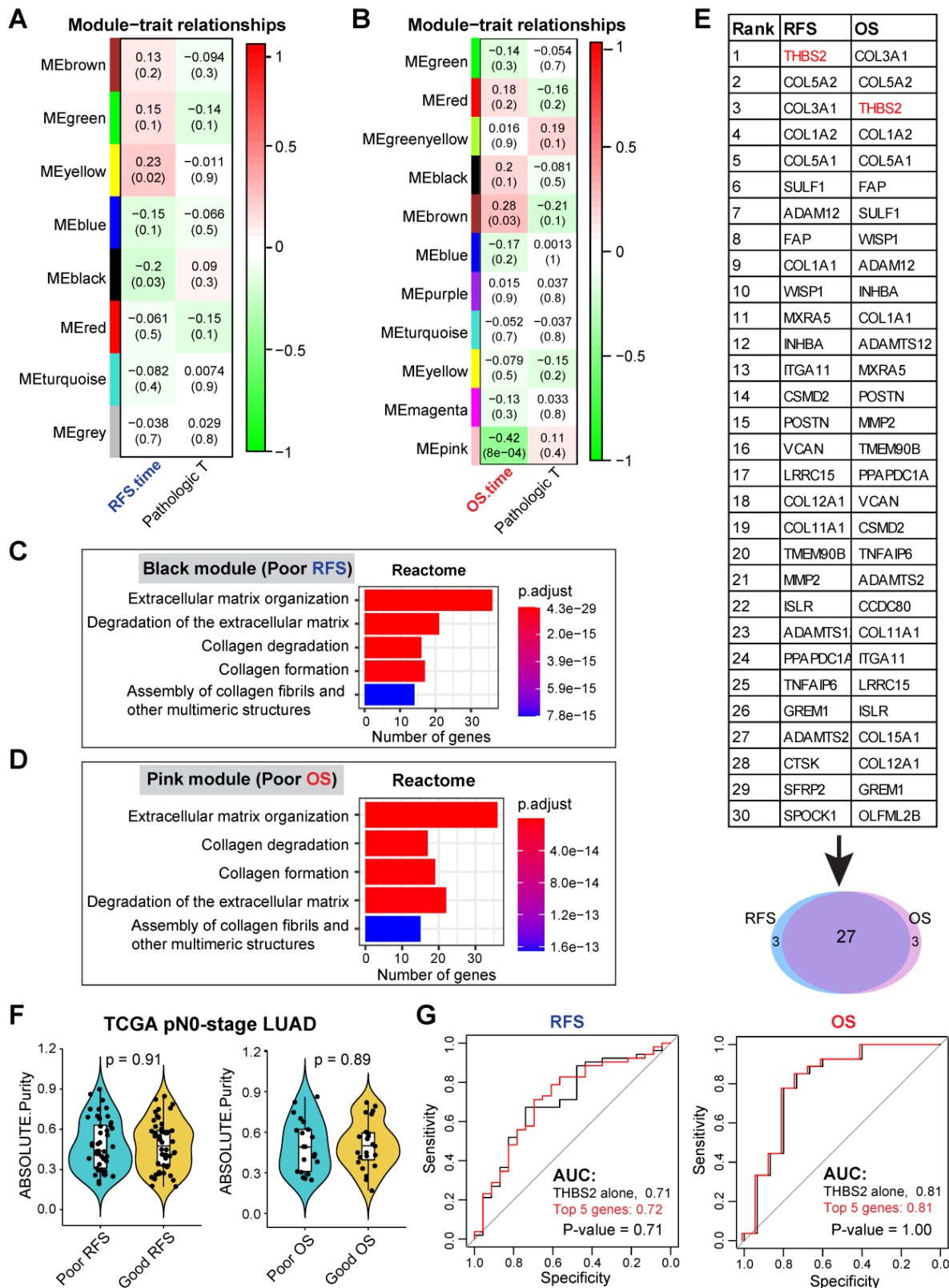


Figure 2. WGCNA analysis identifies THBS2 as a candidate biomarker predictive of RFS and OS in early pN0-stage LUAD. A, B, WGCNA analysis. Consensus network modules correlated with RFS and pathological (p) T-stage (tumor size) in the TCGA LUAD (lung adenocarcinoma) cohort using the eigenmodule (the first principal component of the module). Pearson correlation coefficient along with p-value in parentheses underneath; color-coded according to correlation coefficient (legend at right). The blue color indicates a negative correlation, while the red color represents a positive correlation. C, D, Reactome pathway enrichment analyses of genes in black (related to poor RFS; C) and pink (related to poor OS; D) modules. E, Top 30 connected genes in black (negatively correlated with RFS) and pink modules (negatively correlated with OS). Lower panel: Venn plot showing the overlap between RFS- and OS-related top 30 connected genes. F, The difference in tumor purity between pN0-LUAD patients with good and poor overall survival (OS). The ABSOLUTE-algorithm was used for the estimation of tumor purity, which was directly downloaded from the UCSC portal (<https://xenabrowser.net/datapages/>, TCGA LUAD dataset). P-value was calculated by two-sided student's t-test. G, Comparison of the difference between the receiver operating characteristic (ROC) curves of two predictive models derived from THBS2 alone and the top 5 genes (THBS2, COL3A1, COL5A2, COL1A2, COL5A1), respectively.

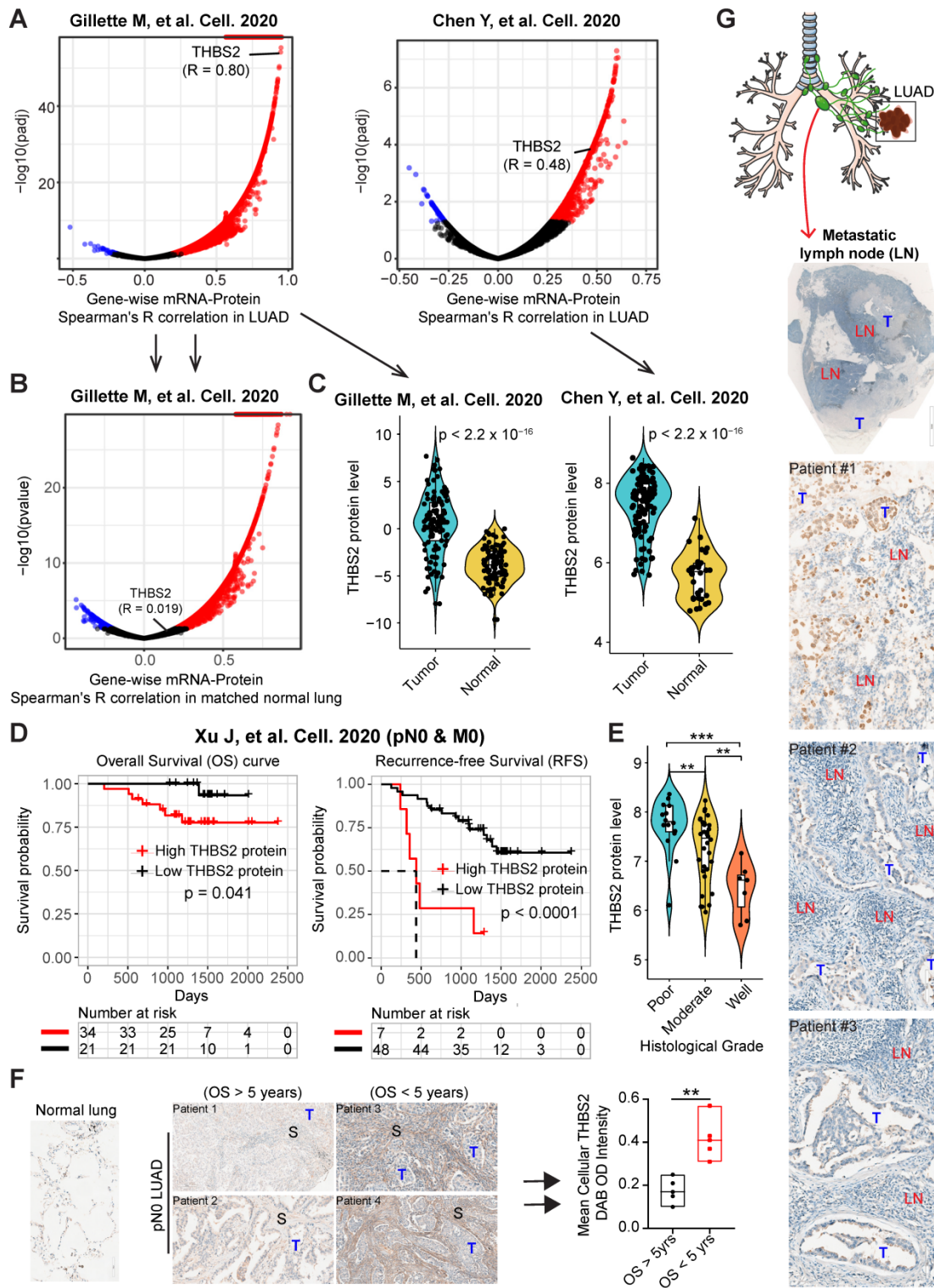


Figure 3. Multiple external and internal validation of THBS2 as a prognostic biomarker. A, B, Genome-wide mRNA-protein correlation (Spearman) analysis in lung adenocarcinoma (LUAD) tumors (A) and matched normal lung tissue (B). The blue color indicates a significantly negative correlation (adjusted $p < 0.01$), while the red color represents a significantly positive correlation. Data were downloaded and reanalyzed from Gillette M, et al. Cell. 2020 and Chen Y, et al. Cell. 2020. C, Violin plots showing the protein level of THBS2 in pN0-stage LUAD compared with matched normal lung tissue. D, The association between THBS2 protein levels and OS and RFS in pN0-stage LUAD. Data were downloaded and reanalyzed from Xu J, et al. Cell. 2020. Of note, only one (Xu J, et al. Cell. 2020) but not the other two datasets (Gillette M, et al. Cell. 2020 and Chen Y, et al. Cell. 2020) provided the survival data. However, in the former dataset (Xu J, et al. Cell. 2020), there was no data of the matched normal lung tissue available. As such, we were only able to show the association of THBS2 protein level with survival with the former dataset, whereas comparing the difference in the THBS2 protein level between the pN0-stage LUAD and matched normal lung tissue with the later two datasets. The clinical information could be found in the Supplementary Table 1 of each publication. E, The association between THBS2 protein level and tumoral differentiation state in pN0-stage LUAD. Data were downloaded and reanalyzed from Xu J, et al. Cell. 2020. Of note, the differentiation stage of tumors is a critical histopathological classification of solid tumors, and is strongly associated with tumor behavior. Generally, tumors with poorer differentiation are more aggressive than their more differentiated counterparts. F, Internal immunohistochemistry (IHC) data showing the location of THBS2 expression in the samples from LUAD patients with short and long survival. ** $p < 0.01$ by two-sided Welch's t-test. Scale bar: 200 μ m. G, Representative IHC showing the positive (upper panel: strong staining; middle/lower panel: moderate/weak staining) staining of THBS2 in three LUAD cases with regional lymph node metastasis. Scale bar: 100 μ m.

Additionally, we retrospectively examined LUAD samples with pathological confirmation of regional lymph node metastasis, which is closely associated with (regional or distant) tumor recurrence and metastasis. Strikingly, we observed that 6 out of 10 tumor-draining lymph nodes samples had proportions, albeit heterogeneous, of metastatic LUAD cancer cells that were THBS2 positive (Figure 3G), in agreement with our findings showing the association of high *THBS2* expression with tumor relapse (Figure 2; Figure S3). Notably, the lymph node represents a critical meeting point of immune cells where adaptive immunity is induced. These lines of evidence support the idea that THBS2 might facilitate tumor recurrence and metastasis, in part, by promoting the escape of immune surveillance in LUAD.

Taken together, the above data reproducibly demonstrated THBS2 as a robust biomarker in predicting the poor prognosis of patients with early pN0-stage LUAD, and high THBS2 expression marks an aggressive phenotype of LUAD.

THBS2 is highly secreted via exosomes by aggressive LUAD tumors

The above evidence revealed THBS2 as a secreted protein (Figure S3B) and also a predictive marker for patients' prognosis and treatment response (Figure 2; Figure 3; Figure S3-S5), which was reminiscent of exosomes that are important mediators of cell-to-cell communication and are associated with drug resistance, as well as tumor recurrence/metastasis [14].

We thus purified exosomes from the tumor tissues and plasma samples of pN0-stage LUAD (N = 5) and healthy controls (N = 5), respectively (Figure 4A, B; Figure S6A, B), and then performed the quantifications of THBS2 exosomes (Figure 4C, D). The data in Figure S6A, B validated the purity of isolated exosomes, based on characterizations of the morphology (transmission electron microscopy), and the size measurement (Nanoparticle Tracking Analysis), and classical exosomal markers (western blot). Our data confirmed the abundance of tissue-derived total (Figure 4B) and THBS2 (Figure 4C) tumor exosomes in lung tumors, compared to the matched normal lung tissue. Particularly, its level was much higher in tumors from patients with short RFS (Figure 4B, C). In parallel, we also detected a higher level of THBS2 exosomes in the plasma of patients with pN0-stage LUAD, compared to that of the healthy controls (Figure 4C). By contrast, there is no difference in the non-exosomal THBS2 or the total THBS2 in the plasma between pN0-stage LUADs and the healthy controls (Figure 4D), highlighting the

promises of the exosomal form of THBS2 in defining an aggressive subset of early-stage LUAD. Besides, we also dissected the specific location of exosomal THBS2, which is closely related to the way it interacts with its target cells (see the discussion). The data demonstrated that THBS2 is located on the membrane rather than inside of LUAD-derived exosomes (Figure 4E).

scRNA-seq analysis reveals subsets of CAFs as a cellular source of THBS2 expression in pN0-stage LUAD

Next, we sought to identify the cellular source of THBS2 expression. Immunohistochemistry (IHC) analysis demonstrated that THBS2 was detectable in cancer cells but prominently in peritumoral stromal cells (Figure S3A; Figure 5A). In our WGCNA analysis, we noted that THBS2 was mostly co-clustered with fibroblast activation protein (FAP) (Figure 2E), a typical marker of fibroblasts, prompting us to hypothesize that CAFs might be a major source of THBS2 production.

Previous evidence highlighted the heterogeneity of CAFs, defining distinct CAF subsets characterized by different molecular profiles, biological functions, and tumor immunological signatures [73, 74]. To investigate whether CAFs are the major source of THBS2 expression and to identify the specific subsets of CAFs, we applied the single-cell RNA sequencing (scRNA-seq) analysis, a powerful tool deconvolving the cell-type composition within tissues and deciphering the transcriptomic profiles of each cell, to two surgical cases with early-stage lung cancer (pT1N0M0) and adjacent normal lung tissues (Figure S7A, B). Notably, in these samples, scRNA-seq data showed a small proportion of CAFs but a large proportion of immune cells (Figure 5B). These observations were partially due to the bias introduced during tissue dissociations, leading to overestimating the immune cell proportions in comparison to the stromal and epithelial cell types [75].

The results demonstrated that THBS2 was mainly expressed by fibroblasts (Figure 5B; Figure S7B), and more importantly, fibroblasts from tumors (CAF) had significantly higher expression of *THBS2* than matched normal lung-derived fibroblasts (Figure 5C). Given the heterogeneity of CAFs [73, 74], we further divided CAFs into 7 subclusters, based on the Clustree algorithm that is used to increase gene representation and achieve optimal cluster separation (Figure S7C) [27], we found that in the two studied lung tumor samples, THBS2 was mainly expressed by four CAF subclusters (2, 3, 4, 5, particularly 2) (Figure S7D, E), suggesting the presence of heterogeneity within THBS2+ CAFs. Furthermore, the top 10

upregulated genes in THBS2+ CAFs, compared with THBS2- CAF subclusters, were (from top 1 to top 10): *THBS2*, *COL3A1*, *BGN*, *COL5A2*, *COL1A1*, *COL6A3*, *FAP*, *CTHRC1* and *SULF1* (Figure 5D).

CAFs are comprised of highly heterogeneous populations [73, 74], and can be generally defined using a panel of typical markers, e.g. FAP, α SMA+ (myofibroblast-like; encoded by *ACTA2*), etc. We then sought to know whether THBS2+ CAFs represent a unique population that is different from CAFs defined by classical markers. Strikingly, based on the scRNA-seq data of CAFs, we observed that THBS2+

CAFs appear to have a drastically different distribution from *ACTA2*+ or *S100A4*+ CAFs (Figure 5E), and THBS2+ CAFs have significantly lower expression of *ACTA2* or *S100A4* than THBS2- CAFs (Figure 5F). Furthermore, co-expression analyses demonstrated that FAP-high CAFs are largely not overlapping with THBS2-high CAFs, and that there is a significant but a weak correlation between FAP and THBS2 across individual CAFs (Figure 5G), although overall THBS2+ CAFs have higher expression of FAP than THBS2- CAFs (Figure 5F).

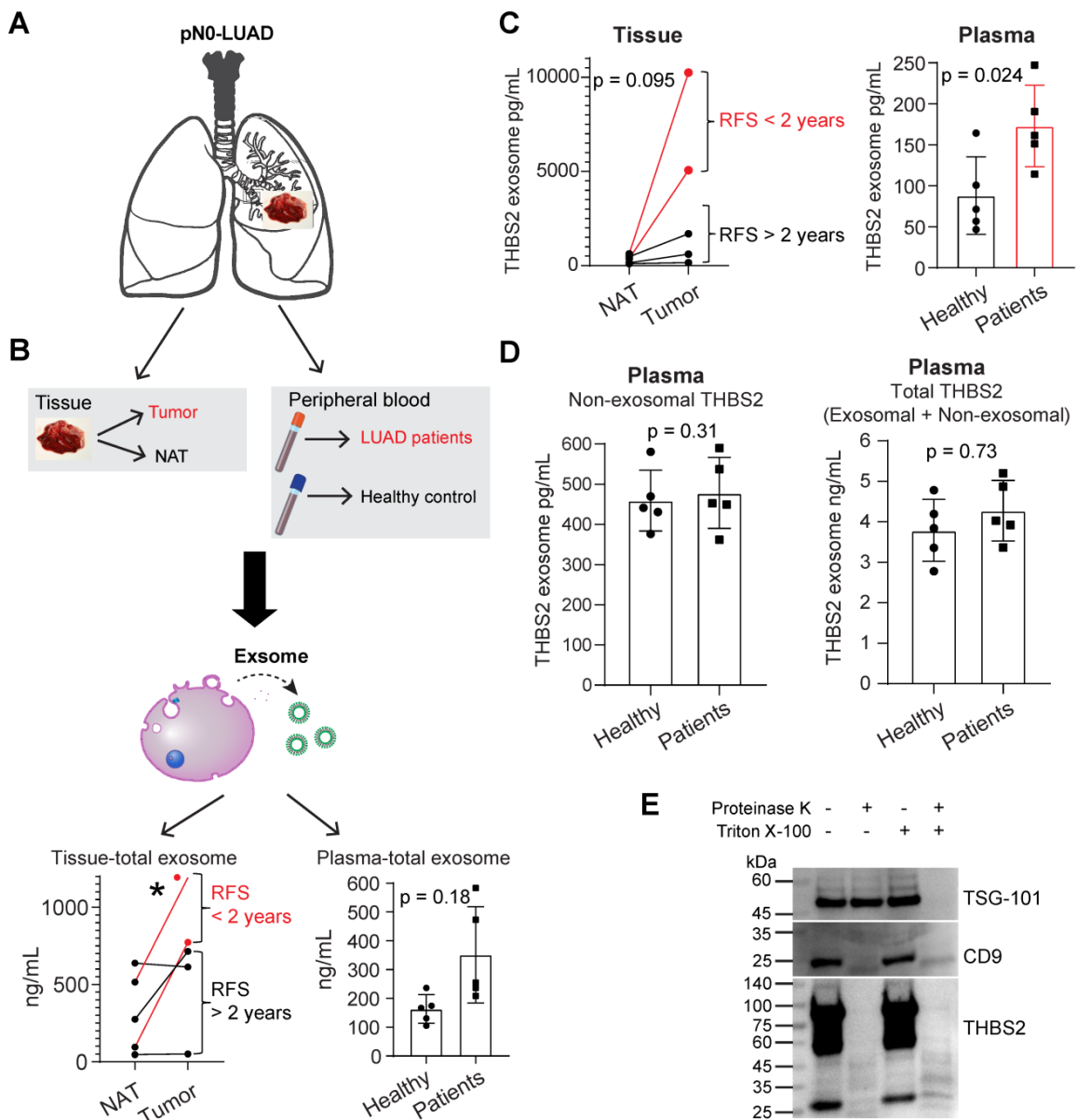


Figure 4. Identifying secreted THBS2 as an exosome protein. A, Exosome isolation, purification and characterization. In A, lung tissue (primary lung adenocarcinoma (LUAD, N = 5); normal adjacent lung (NAT, N = 5)) and blood plasma samples (from LUAD, N = 5; from healthy controls, N = 5) were included. B-D, The quantitation of purified total (B) and THBS2 (C) exosome proteins of lung tissue and plasma samples; P-value ($*p < 0.05$) was calculated using two-sided paired (left panel) or unpaired (right panel) t-test. (D), The difference in the amount of non-exosomal (left panel) and total (exosomal plus non-exosomal; right panel) THBS2 protein between plasma from LUAD and healthy controls (N = 5 for each group). P-value was calculated using two-sided unpaired t-test. E, Dissecting the specific location of exosomal THBS2 using proteinase K assay. 20 mL plasma of 6 LUAD patients were used to purify exosomes (500 μ L; concentration: 1062 ng/ μ L), and were then incubated in PBS (control), proteinase K alone, Triton X-100, or combined proteinase K plus Triton X-100, respectively. These samples were then subjected to immunoblot. TSG-101, a typical exosomal intra-membrane protein, and CD9, a classical exosomal trans-membrane protein, were used as positive controls. Notably, THBS2 was detected only in the membrane but not inside of the exosomes.

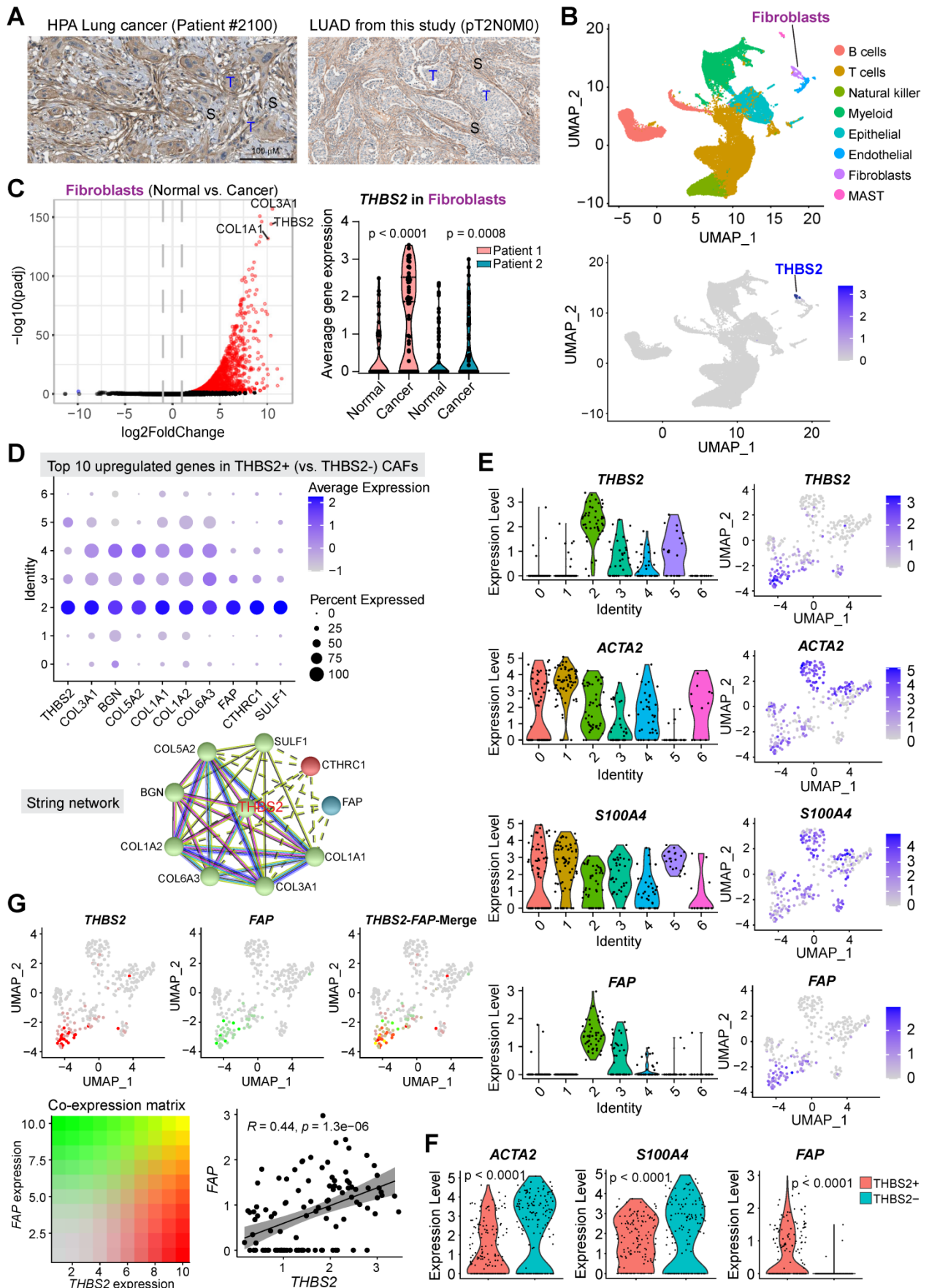


Figure 5. scRNA-seq analysis reveals subsets of CAFs as the major source of THBS2 production. A, Immunohistochemistry/hematoxylin staining showing the expression of THBS2 in LUAD samples from TCGA and this study. Of note, THBS2 was detected in cancer and more predominantly in peritumoral stromal cells. Scale bar: 100

µm. B, UMAP (Uniform Manifold Approximation and Projection) plot showing the expression of *THBS2* across different cellular subpopulations from lung tumors (pTINOM0, N = 2) and matched normal lung tissue (N = 2). Of note, high *THBS2* expression was from fibroblasts based on annotation (see Figure S7B). C, Volcano plot (left panel) showing the differentially expressed genes between fibroblasts from lung primary tumors and normal adjacent lung tissue. Of note, *THBS2* was listed as the top genes upregulated in from fibroblasts from lung primary tumors, compared with those from matched normal lung tissue. In the right panel, the violin plots showing that *THBS2* was upregulated in lung primary tumors compared to normal adjacent lung tissue across two individuals. The significance was determined using two-sided Student's t-test. D, The upper panel showing the top 10 genes of *THBS2*+ compared with *THBS2*- CAFs across the 7 CAF subclusters. The lower panel showing the String interaction network of the top 10 genes. In the String network, the interactions were clustered (N = 3; represented by 3 colors) based on kmeans clustering algorithm. E, Violin (left) and UMAP (right) plots showing *THBS2*, *ACTA2*, *S100A4*, or *FAP* expression across different CAF subclusters. Of note, *THBS2* was mainly expressed by cluster 2-, 5-, 3 and 4-annotated CAFs. F, Violin and UMAP plots showing the difference in the expression of *ACTA2*, *S100A4*, or *FAP* between *THBS2*+ and *THBS2*- CAFs. P-value calculated by two-sided unpaired t-test. G, UMAP plots showing the co-expression of *THBS2* and *FAP* across individual single CAFs. Red/green dots represent CAFs expressing *THBS2*+ only/*FAP*+ only (upper left/middle panels), respectively, and yellow dots indicate CAFs co-expressing *THBS2* and *FAP* only (upper right panel); lower left panel showing the co-expression matrix across CAFs with different expression of *FAP* and *THBS2*; lower right panels showing the correlation (Pearson) between *THBS2* and *FAP* across *THBS2*+ CAFs. (1) Strong correlation: Pearson's $r \geq 0.8$; (2) Moderate: $0.5 \leq$ Pearson's $r < 0.8$; (3) Weak: $0.3 \leq$ Pearson's $r < 0.5$; (4) No correlation: Pearson's $r < 0.3$. The darker the color, the higher the expression level of the indicated markers. Of note, only a minority of CAFs co-express high *THBS2* and *FAP*.

Additionally, we mined public datasets relating to scRNA-seq analysis of non-small cell lung cancer (NSCLC) samples from TISCH, a comprehensive web resource enabling interactive single-cell transcriptome visualization of the TME [76]. The analyses also revealed that *THBS2* was consistently expressed by CAFs (Figure S7F). Moreover, these observations also held true in other organs-derived tumors (e.g., breast invasive carcinoma [BRCA], Head and Neck squamous cell carcinoma [HNSCC], ovarian serous cystadenocarcinoma [OV], pancreatic adenocarcinoma [PAAD], Bladder Urothelial Carcinoma [BLCA] sarcoma [SARC]) that are generally characterized by a high ECM/stromal signature and poor response to immunotherapy (Figure S8) [77]. The above evidence suggested that *THBS2* expression is mainly derived from CAFs, which is independent of organ lineage.

Collectively, these data indicated that *THBS2*+ CAFs represent a unique subpopulation that did not co-cluster with CAFs defined by typical markers.

THBS2-high LUAD is characterized by a high ECM/stromal signature together with suppressive tumor immunity

To investigate the biological functions of *THBS2* in LUAD, we analyzed the molecular features of *THBS2*-high LUAD samples. Based on the RNA-sequencing data of TCGA pN0-stage LUAD, we observed that *THBS2*-high LUAD tumors were characterized by enrichment for PI3K-AKT, focal adhesion, proteoglycan ECM-receptor interaction, and protein/collagen metabolic pathways/process, positive regulation of cell motility, and stromal signature (Figure 6A-C). Similarly, reverse phase protein array (RPPA) data (including 216 tumorigenesis-associated proteins) of TCGA pN0-stage LUAD showed that *THBS2*-high LUAD tumors are mostly characterized by a high level of fibronectin, a typical mesenchymal marker, and low level of several classical epithelial biomarkers, E-cadherin, ERBB3 and Claudin-7 (Figure 6D). These analyses *THBS2*-high LUAD is characterized by a high ECM/stromal signature that marks a mesenchymal-like phenotype and is typically

associated with tumor metastasis and therapy resistance.

In comparison with the scRNA-seq profilings of *THBS2*- CAFs, gene set enrichment analysis (GSEA; Hallmark module) revealed that *THBS2*+ CAFs were significantly enriched for signatures of the epithelial-to-mesenchymal transition (EMT), immune-inflammatory response (e.g., TNF α -NF κ B, IL6-JAK-STAT3, IL2-STAT5, inflammatory response; complement, interferon-gamma response, allograft rejection), hypoxia, TGF- β and glycolysis signaling pathways (Figure S9), suggesting a pleiotropic role and an immune-inflammatory phenotype of *THBS2*+ CAFs.

Considerable evidence has revealed that tumors with a high stromal signature are prone to immune evasion and resistance to immunotherapy and that tumor-derived glycoproteins endow immunosuppressive functions [78]. Intriguingly, based on curated immune subtype models [58], our analysis showed that pN0-stage LUAD tumors with high *THBS2* gene expression were enriched for TGF-beta Dominant and Wound Healing immune subtypes but reduced for Inflammatory subtypes (Figure 6E). In support of this, based on the proteomics data of pN0-stage LUAD tumors [50], *THBS2* protein level was significantly negatively correlated with the antitumor immune score (Figure 6F). These lines of evidence reinforced the notion that *THBS2*-enriched TME might facilitate immune escape (Figure 3G).

Multiplexed IHC (mIHC) staining analysis revealed the spatial expression of THBS2 and its interaction with TIME

Next, we investigated the interaction between *THBS2* and tumor immune microenvironment (TIME) by implementing mIHC staining analysis that enables simultaneous multiparametric readouts at the single-cell level from a single tissue section. First, to confirm the spatial expression of *THBS2* (Figure 5E-G), we performed mIHC analysis by co-staining *THBS2* and three typical CAF markers (*FAP*, α SMA and *S100A4* [also known as *FSP-1*]) (Figure 7A), the results confirmed that *THBS2* and the three classical CAF markers were mainly expressed in peritumoral

stromal compartments (Figure 7B). Overall, in the tested LUAD (pT2bN0M0) samples, the percentage of THBS2+ CAFs was much higher than that of FAP+, αSMA+ or S100A4+ CAFs in the peritumoral stromal compartments (Figure 7B, C). Notably, only a minority of THBS2 overlapped with the three classical CAF markers (Figure 7D-E), supporting that THBS2+ CAFs represent a unique subset, which was in line with the above scRNA-seq data (Figure 5E-G).

In parallel, our findings were examined in a resected sample with lung squamous cell cancer (LUSC, pT2bN0M0) that has the same histological grade (moderate) and similar genetic backgrounds (no common oncogenic mutations in NSCLC) (Figure S10A-E), given that there is a dramatic difference in

the TME between LUAD and LUSC [79]. In contrast to LUAD, the percentage of THBS2+ CAFs in the LUSC sample was much lower than that of FAP+, αSMA+ or S100A4+ CAFs in peritumoral stromal compartments (Figure S10C). Similar to LUAD, only a few THBS2 overlapped with the three classic CAF markers in the LUSC sample (Figure S10D, E). Based on the TCGA NSCLC cohort, pN0-stage LUSC tumors have significantly higher THBS2 than the LUAD counterparts (Figure S10F). Concerning patient prognosis, high THBS2 expression also predicted poor survival in pN0-stage LUSC after surgery (Figure S11). Whether the biological functions of THBS2 in LUAD differ from those in LUSC warrants further study.

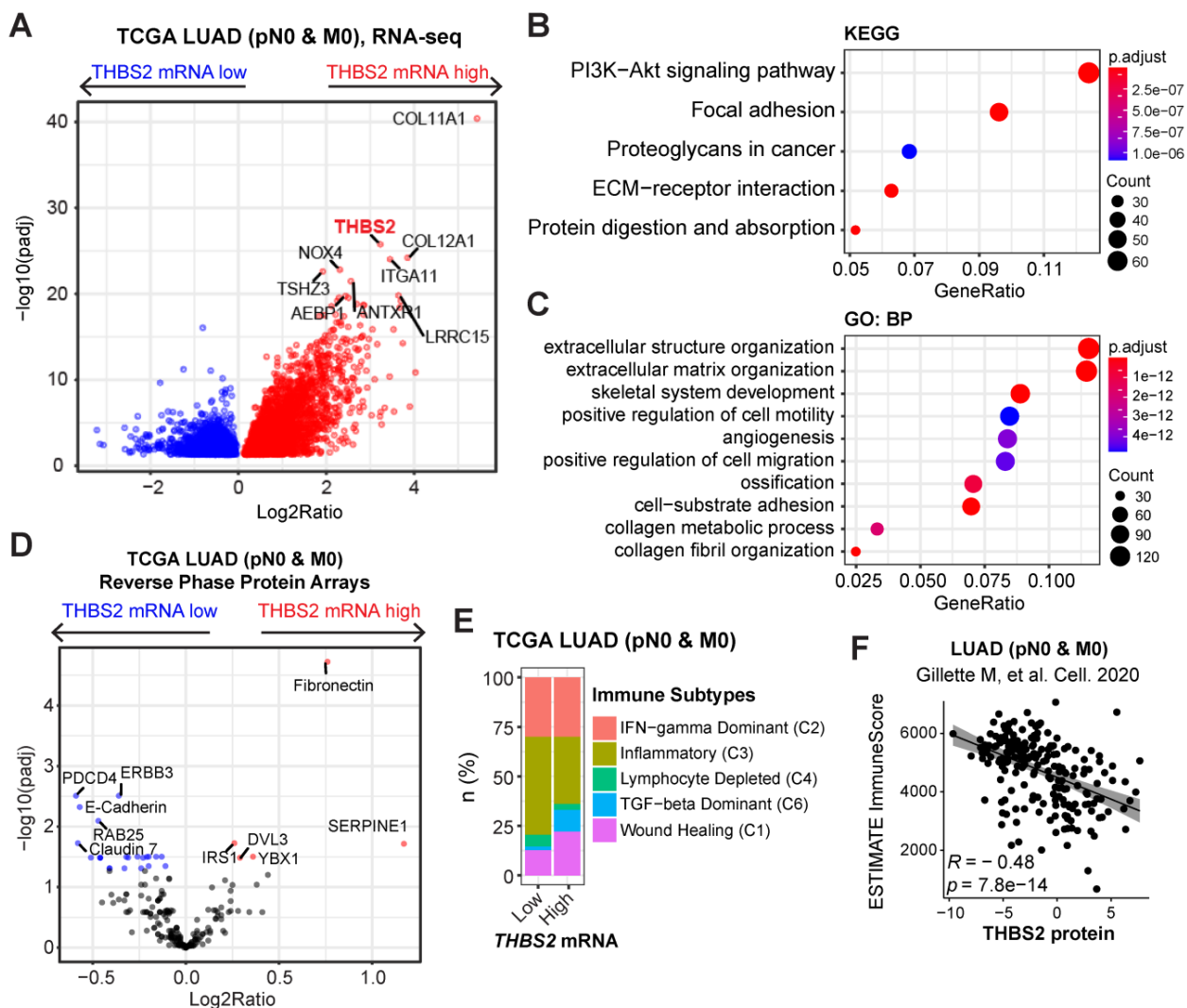


Figure 6. LUAD tumors with high THBS2 expression are characterized by an enriched ECM/stromal signature and dysregulated tumor immunity. A-C, Pathway enrichment in THBS2-high LUAD compared with THBS2-low LUAD. A, Volcano plot showing the upregulated genes in THBS2-high LUAD. Data were from TCGA pN0-stage LUAD. B, C, KEGG (Kyoto Encyclopedia of Genes and Genomes; B), and GO-BP (Gene Ontology Biological Processes; C) pathway analyses were performed based on A. D, Differentially expressed proteins between THBS2 (mRNA)-high and THBS2-low LUAD based on A. The blue color indicates the significantly downregulated proteins (adjusted $p < 0.01$), while the red color represents the significantly upregulated proteins in THBS2-high LUAD. Data were downloaded and reanalyzed from the TCGA LUAD RPPA (reversed-phase protein array) dataset (see the details in Methods). E, Difference in the distribution of immune subtypes (C1-C6) between THBS2-high and THBS2-low LUAD based on A. The genes contained in each signature were evaluated using model-based clustering by the “mclust” R package. Each sample was finally grouped based on its predominance with the C1-C6 signature. The immune subtype models were based on Thorsson V et al. Immunity. 2018 (See the methods). F, The correlation between the antitumor immune score and THBS2 protein level across pN0-stage LUAD. Data of antitumor immune score and THBS2 protein level were downloaded and reanalyzed from the Supplementary Tables published in Gillette M, et al. Cell. 2020.

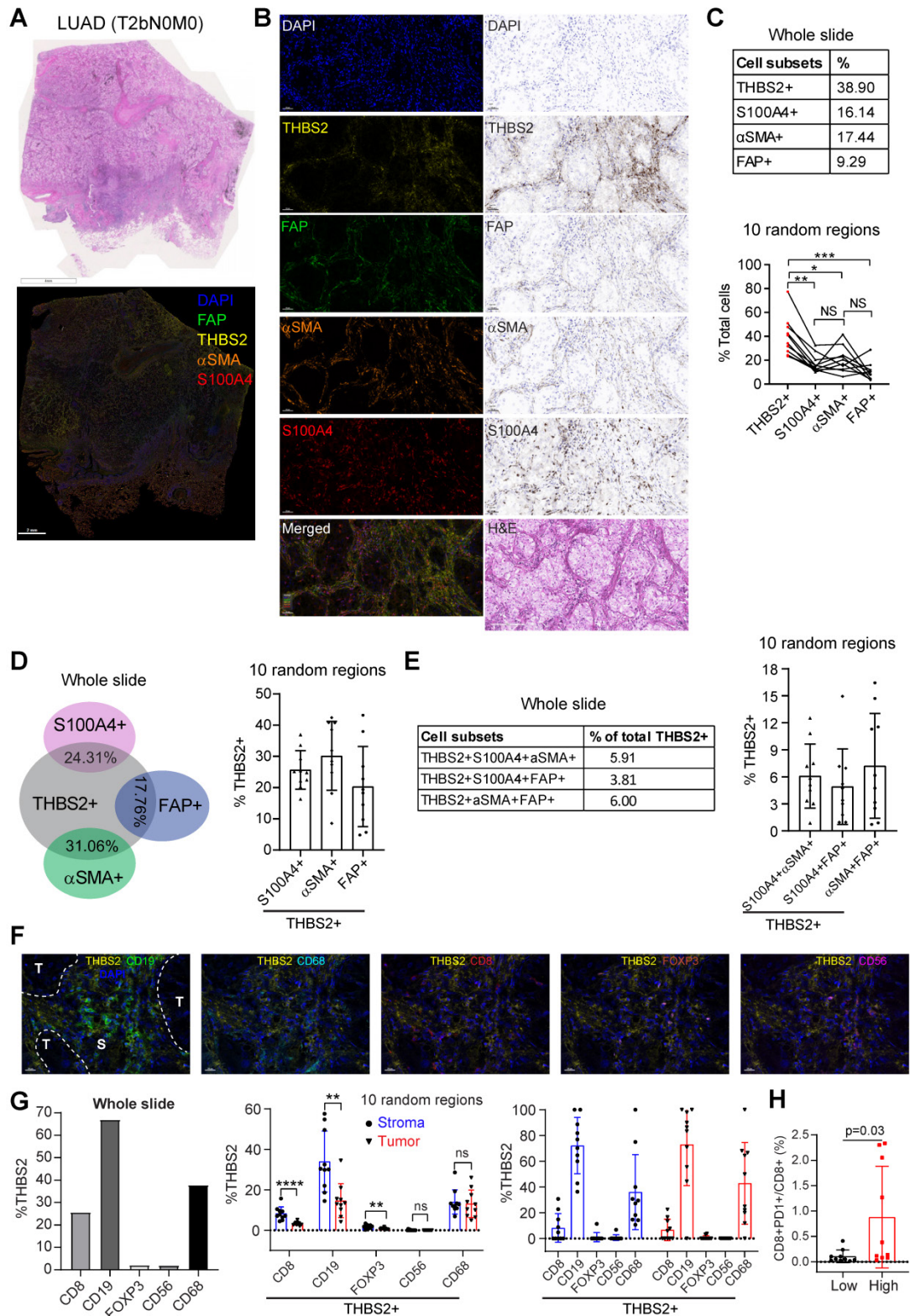


Figure 7. Multiplexed IHC shows the spatial association between THBS2 and typical CAF markers in LUAD. A, B, THBS2 co-staining with three classical CAF markers (αSMA, FAP, S100A4 [FSP1]) in a resected LUAD (lung adenocarcinoma) (pT2bN0M0) sample. The image acquisition of all markers occurred simultaneously. Panel A shows the whole slide scan; panel B shows the representative regions (200x). Scale bar: 50 μm. C–E, Individual or selected combinations of THBS2 and three classical CAF markers (αSMA, FAP, S100A4 [FSP1]) markers (whole slide and 10 randomly selected regions) were quantified and shown. Single-staining (THBS2, αSMA, FAP, or S100A4; C), double-staining (THBS2/αSMA, THBS2/FAP, or THBS2/S100A4; D), triple-staining (THBS2/αSMA/ FAP, THBS2/FAP/S100A4, or THBS2/αSMA/S100A4; E) were quantified by using HALO® software (Please see the detailed description in the Methods section “Image acquisition and data quantification”). **p* < 0.05; ***p* < 0.01; ****p* < 0.0001 by paired ANOVA test. F, G, Indicated combinations markers (whole slide [left] and 10 randomly selected [under 50x magnification] regions [middle and right]) were quantified and shown. The upper panel (F) showed the representative regions (400x). In tumor and stromal compartments within the 10 different regions, the expression of indicated markers was quantified and compared, respectively. ***p* < 0.01; ****p* < 0.0001 by two-sided student’s *t*-test. Scale bar: 20 μm. H, Ratio of CD8+PD1+ to total CD8+ T cells in 10 randomly (5 tumoral and 5 stromal regions) selected regions of a LUAD tumor from A (related to Figure S15C). We performed multiplexed IHC with CD4, CD8, CD19 and PD-1 (5-Color Multiple IHC Kit) from a serial slide of the same tumor as Figure 7A–G. *p*-value was calculated using paired student’s *t*-test.

Our above evidence revealed a potential link of THBS2 with TIME. CD36 and CD47 are two well-characterized receptors of secreted THBS2 [80]. Interestingly, recent studies demonstrated that CD36 was selectively upregulated intratumoral regulatory T (Treg) cells [81] and promoted intratumoral CD8+ T cell dysfunction [82]. Thus, targeting CD36 could enhance the response to immunotherapy [81, 82]. Similarly, CD47, which promotes immune evasion by engaging signal-regulatory protein alpha (SIRP α) and serves as an inhibitory receptor on macrophages, is emerging as a novel macrophage immune checkpoint for cancer immunotherapy [83]. Our scRNA-seq profiling together with the mining data showed that CD36 was mainly expressed by monocytes/macrophages while CD47 was broadly expressed particularly by cancer cells (**Figure S12A, B**). More intriguingly, inferring cell-cell communication using the CellChat algorithm revealed THBS2+ CAFs have more profound interaction weights with both tumor and immune cells compared with THBS2- CAFs based on our scRNA-seq of two pT1N0M0 lung cancer samples (**Figure S13A**). Further, the ligand-receptor analysis showed THBS2-CD47 was likely to contribute mostly to the ligand-receptor-based interactions (**Figure S13B**). Among the top enriched signaling pathway network (**Figure S13C**), the interactions between THBS2+ CAFs and other cells within the tumor micro-ecosystem were most mediated by THBS, followed by stromal/immune signaling pathways, e.g. THY-1, FN-1, TGF- β , IL6/4, MHC-I, VEGF, CD40, or TIGIT. These data suggest a pleiotropic role of THBS2 in the TME of early-stage LUAD. Since our above evidence demonstrated that THBS2 could be shuttled in the form of non-exosome and exosomes, thus supporting that THBS2 can interact with immune cells via ligand-receptor recognition or vesicle uptake, consequently affecting their respective functions.

We further co-stained THBS2 with markers of cytotoxic T (CD8), Treg (FoxP3) and B (CD19) lymphocytes, as well as tumor-associated macrophages (CD68) [84] and nature killer (NK) cells (CD56) [85], which showed that immune cells were mainly located at the stromal compartment (**Figure 7F; Figure S14A**). Strikingly, among the biomarkers examined, CD19, followed by CD68 and CD8, were the most co-stained markers with THBS2 (**Figure 7F, G**), suggesting that THBS2 mainly impacts B cells, macrophages and CD8+ T cells within TIME, thus potentially modulating tumor immunity via interacting with these immune cells. Additionally, THBS2-expression high compartments were associated with elevated percentage of CD8+PD1+ ($p=0.03$), CD4+PD1+ ($p=0.07$), and CD19+PD1+

($p=0.14$) lymphocytes (**Figure 7H; Figure S14B; Figure S15D**), indicating that THBS2 might promote exhaustion of these infiltrated immune cells. Furthermore, quantification of immune cell infiltrates revealed a significant decrease in CD8+ T cells (**Figure 8A-C; Figure S15A, B**), to a less extent in CD19+ B cells accompanied by high THBS2 expression (**Figure 8B, C; Figure S15B, C**). In agreement, estimation of the immune cell infiltrates, using quanTIseq, an algorithm specifically developed for RNA-sequencing data [60], showed a significantly negative correlation between CD8+ T cell infiltrates and THBS2 expression across TCGA LUAD samples (**Figure 8D**). There is also a correlation, albeit to a less extent, between THBS2 expression with other immune cell infiltrates (**Figure 8D**). Together, these data support a suppressive role of THBS2 in modulating TIME; however, how THBS2 exactly affects these immune cells remains to be further elucidated.

THBS2-high LUAD displays a poor response to clinical immunotherapy

The above evidence revealed a suppressive TIME in THBS2-high LUAD, prompting us to investigate the association between THBS2 expression and the response to clinical immunotherapy.

First, we performed integrative analyses of the transcriptomic and therapeutic response data of 20 BALB/c mice inoculated subcutaneously with AB1-HA cells and treated with anti-CTLA4 therapy (GSE63557) [57], and intriguingly, tumors from non-responders had significantly upregulated THBS2 expression (**Figure 9A**). Second, along the same line, mining two independent datasets that contain lung cancer (GSE135222) or melanoma (GSE78220) patients treated with anti-PD1/PD-L1 immunotherapies, we observed that higher THBS2 expression was associated with poor response and short PFS/OS after immunotherapy (**Figure 9B, C**). Additionally, we retrospectively reviewed THBS2 expression in the pre-immunotherapy biopsies of LUAD patients ($N = 13$) who subsequently received anti-PD-1 immunotherapy after the failure of first-/second-line treatment. Remarkably, low expression of THBS2 was significantly associated with a better response to immunotherapy (**Figure 9D**). Finally, we integrated the recently established four TME subtypes that deciphered the abundance of both malignant and non-malignant cell subpopulations and the activity of tumor-promoting and tumor-suppressive processes occurring within a tumor [59]. This new classification model demonstrated robustness in identifying subsets responding to immunotherapy. We applied the four TME subtypes to the above lung cancer patient cohort receiving immunotherapy (GSE135222) and observed

that THBS2 expression was significantly positively correlated with Angiogenesis-Fibrosis subtype (mainly derived from the CAF signature) and EMT signature (Figure S16). In contrast, THBS2 expression was significantly negatively correlated with the

antitumor immune microenvironment (specifically effector T cells and NK cells) (Figure S16). Consistently, in TCGA pN0-stage LUAD, high THBS2 expression was associated with more Fibrotic but less Immune-enriched TME subtypes (Figure 9E).

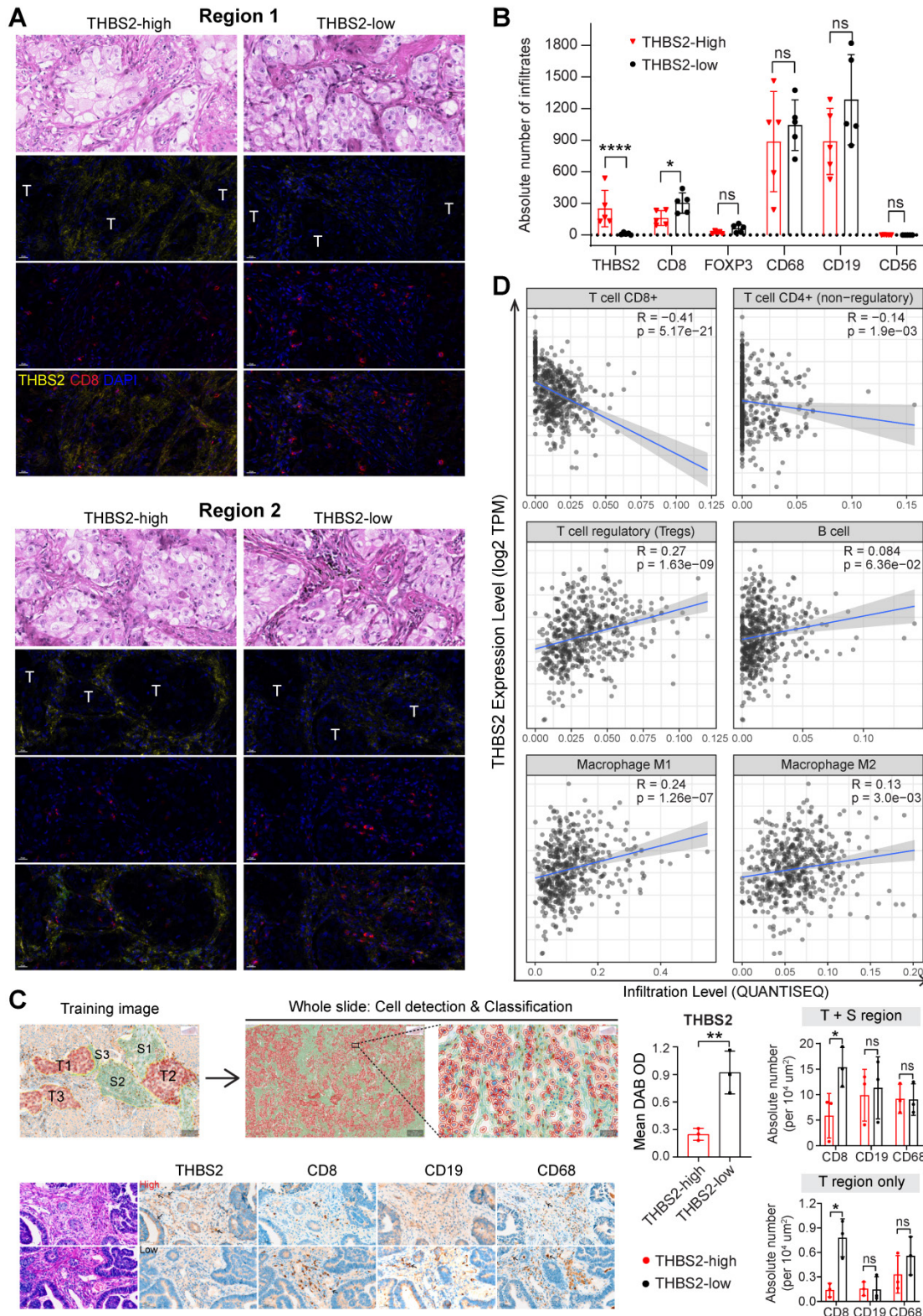


Figure 8. The association between THBS2 expression and immune infiltrates in LUAD. A, B, Panel A showing the representative images of THBS2 co-staining with CD8 T lymphocytes in two regions (THBS2-high and -low) of a resected LUAD (lung adenocarcinoma) (pT2bN0M0) sample. The image acquisition of all markers occurred

simultaneously with the representative regions were shown (200x). Panel B showing the quantification (absolute number of the indicated positive cells) of 5 random regions (under 50x). The quantification of THBS2 level in the first barplot was shown to confirm the difference in the expression of THBS2 between THBS2-high and -low groups * $p < 0.05$; *** $p < 0.0001$ by two-sided student's t-test. ns, not significant. Scale bar: 20 μm . C, An independent pN0-stage LUAD cohort (N = 6) was used to compare the difference in immune cell infiltrates between THBS2-high (N = 3) and -low (N = 3) groups. Left upper panels showing the tumor (T, in red) and stromal (S, in blue) cells (100X), which were used for training to recognize the differential features between tumor and stromal cells (using QuPath software, version 0.3.2). Then the established unique parameters of tumor and stromal cells were applied to the entire slide (left lower). Left lower panels showing the representative IHC images (200x, left). The right panels showing the quantifications of the indicated protein markers. * $p < 0.05$; ** $p < 0.01$ by two-sided student's t-test. ns, not significant. Scale bar: 50 μm . D, Correlation between THBS2 expression and immune infiltrates across p-N0 stage LUAD from TCGA cohort.

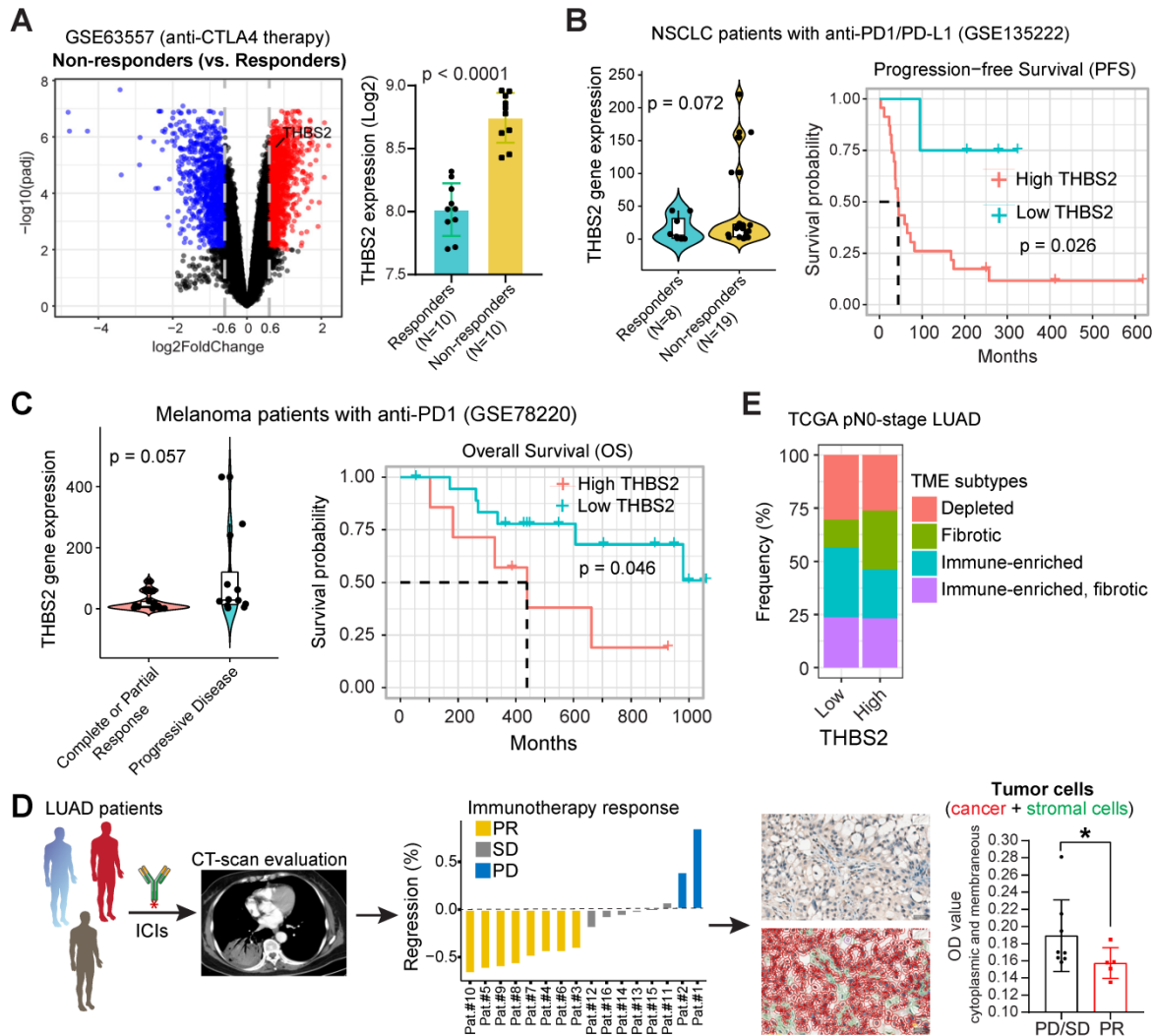


Figure 9. THBS2 expression effectively predicts the response to immunotherapy in clinical patients. A, Differentially expressed genes between the tumors that respond and do not respond to anti-CTLA4 immunotherapy. A barplot was shown to the right specifically illustrating the difference between the responders and non-responders. Of note, THBS2 was significantly highly expressed in tumors that did not respond to anti-CTLA4 immunotherapy. Data were downloaded and reanalyzed from the GSE63557 dataset. B, C, External cohorts validating the association between THBS2 expression in pretreated tumor samples and anti-PD1/PD-L1 therapy from non-small cell lung cancer (NSCLC) (GSE135222; B) and melanoma (GSE78220; C) cohorts. The left panel showed the difference in THBS2 expression between the responders and non-responders; the right panel shows the association of THBS2 in pretreated samples with PFS of patients in this cohort. In the melanoma cohort, the data of patient 16 were excluded because of the on-treatment biopsy. Of note, in the left panel of B, the dashed line was used to highlight that in this studied cohort, the tumors whose baseline expression of THBS2 > 50 all belong to the non-responders group. However, in the right panel, the THBS2 expression in the survival plot was grouped based on the optimal cutoff value determined by R software (see the Methods), but not the dashed line. Likewise, a similar group strategy was used in the two panels of Figure 9C. D, The workflow showing the evaluation of responses to immune checkpoint inhibitors (ICIs) in LUAD patients. After at least two cycles of ICIs, the therapeutic response was evaluated by using computed tomography (CT) scans based on the guideline of RECIST 1.1 (see the Methods). Immunohistochemistry-based quantifications (using QuPath software, see the methods) showing the association between THBS2 expression in pretreated LUAD biopsies and therapeutic response to anti-PD1 immunotherapy. PR: partial response; SD: stable disease; PD: progressed disease. Of note, we acquired a total of 16 patients' samples (middle panel), of which, 3 samples from the PR group could not be evaluated due to the small size and poor quality of the biopsies. As a result, we could not collect the quantification data from these 3 samples, and only 13 samples were finally included for analysis. Scale bar: 20 μm . E, Difference in the distribution of the tumor microenvironment signature (from Bagaev A, et al. Cancer Cell. 2021) between THBS2-high and THBS2-low tumors based on pN0M0-stage TCGA LUAD.

Together, these lines of evidence suggested that LUAD tumors with high expression of THBS2 are prone to immune escape and resistance to immunotherapies.

THBS2 suppresses ex vivo T cell proliferation and promotes tumor growth and metastasis in LUAD xenografts

Because THBS2 is a protein secreted by CAFs

into the tumor microenvironment and correlates with tumor recurrence, we treated cancer cells with exogenous recombinant THBS2 protein to mimic the effect of THBS2 on LUAD cancer cells and T cells isolated from a LUAD patient. *In vitro* transwell migration assays showed that the presence of THBS2 (50 ng/mL, the average level in the serum of patients with early-stage lung cancer [64]) dramatically facilitated the migration of LUAD cells (**Figure 10A; Figure S17A**), although THBS2 does not promote their proliferation (**Figure S17B**). Besides, co-incubation with THBS2 for 96h (200-500 ng/mL, lower than the maximum level secreted by aggressive LUAD tissue (**Figure 4C**)) suppressed the *ex vivo* proliferation of isolated and activated CD3+ T cells from a LUAD patient (**Figure 10B**). In addition, we subcutaneously co-injected THBS2 recombinant protein together with human LUAD A549 cells into immune-deficient nude mice (**Figure 10C**) and mouse LLC cells into immune-competent C57BL/6 mice (**Figure S17C**), which promoted a significant increase in tumor growth and distant micro-metastasis to the lung, compared with the control group (**Figure S17D**). The potentially pleiotropic roles of THBS2 in the micro-ecosystem of LUAD were summarized in **Figure 10D**.

Discussion

pN0-stage LUAD represents a heterogeneous population. Although the primary tumor is radically resected at an early stage, a subset of patients has a high incidence of tumor relapse, resulting in compromised survival [86]; however, little is known about the underlying molecular underpinnings. Furthermore, there is little knowledge about the best strategy, e.g., chemotherapy, radiotherapy, targeted therapy or immunotherapy, to manage this high-risk subset following surgery, and whether additional therapeutic interventions are needed remains controversial [8-11]. These dilemmas underscore the need to understand the cellular and molecular mechanisms in primary lesions that are prognostic for recurrence and as biomarkers as well as potential targets for intervention. Here, based on the integrated multi-omics data, our study demonstrated that THBS2, preferentially secreted via exosomes by a specific subset of CAFs within lung tumors, represents a promising molecular biomarker to stratify the high-risk subset of patients with pN0-stage LUAD after curative surgery. Besides, our evidence revealed a major role of THBS2+ CAFs in modulating the TIME, consequently conferring an aggressive phenotype.

THBS2 is a disulfide-linked homotrimeric glycoprotein that mediates cell-to-cell and cell-to-

matrix interactions. It has been reported that THBS2 is a prognostic biomarker, either poor or good, in a variety of human cancers, including lung cancer [67-69]. THBS2 has been largely described as a serum diagnostic biomarker, particularly in pancreatic cancer, which is characterized by high stromal compartments [66]. Furthermore, recent evidence detects THBS2 as a cancer-specific exosome protein [87]. Additionally, previous evidence revealed the promise of THBS2 as a candidate diagnostic biomarker for early-stage lung cancer [64]. In this study, we particularly showed that THBS2 was preferentially secreted via exosomes by the lung tumors displaying a high aggressive phenotype (**Figure 4; Figure S6**), thereby suggesting exosomal THBS2 as a biomarker defining the high-risk subset of LUAD patients at an early stage. Besides, our data also showed that high expression of THBS2 predicts poor survival in pN0-stage LUAD patients treated with adjuvant chemotherapy or EGFR-TKIs, suggesting that this high-risk subset might not be able to benefit from conventional treatment strategies and that novel treatments are needed. Collectively, the evidence from the literature and our study highlights the promise of THBS2 in the early detection of LUAD, dynamically monitoring tumor recurrence and predicting prognosis, as well as facilitating the decision-making of adjuvant therapy management after curative surgery.

Previous evidence did not dissect which exact cellular subtypes within the tumor micro-ecosystem contribute to the production of THBS2. We provided the first evidence showing that THBS2 was mainly derived from specific subsets of CAFs, informed by the scRNA-seq data, which were different from subsets defined by canonical CAF markers (**Figure 5E-G; Figure S7**). CAFs are the major player promoting therapy resistance and tumor progression. Recently, mounting evidence has highlighted the high heterogeneity of CAFs [73, 74], which play tumor-promoting roles or tumor-restraining functions, highlighting the need to design subtype-specific therapies. Notably, no single marker can define the full CAF populations. A growing list of markers, e.g., α SMA, S100A4/fibroblast specific protein 1 (FSP-1), FAP and so on, have been used to define activated CAFs. Thus, different markers defined distinct CAF subsets with their unique gene signatures and functions [73, 74]. In this study, our work supports that THBS2+ CAFs are mainly expressed in a few subclusters of CAFs and might represent a unique CAF subset that is different from classical CAFs defined by FAP, FSP-1 and α SMA. Whether THBS2+ CAFs have different biological functions remains to be defined.

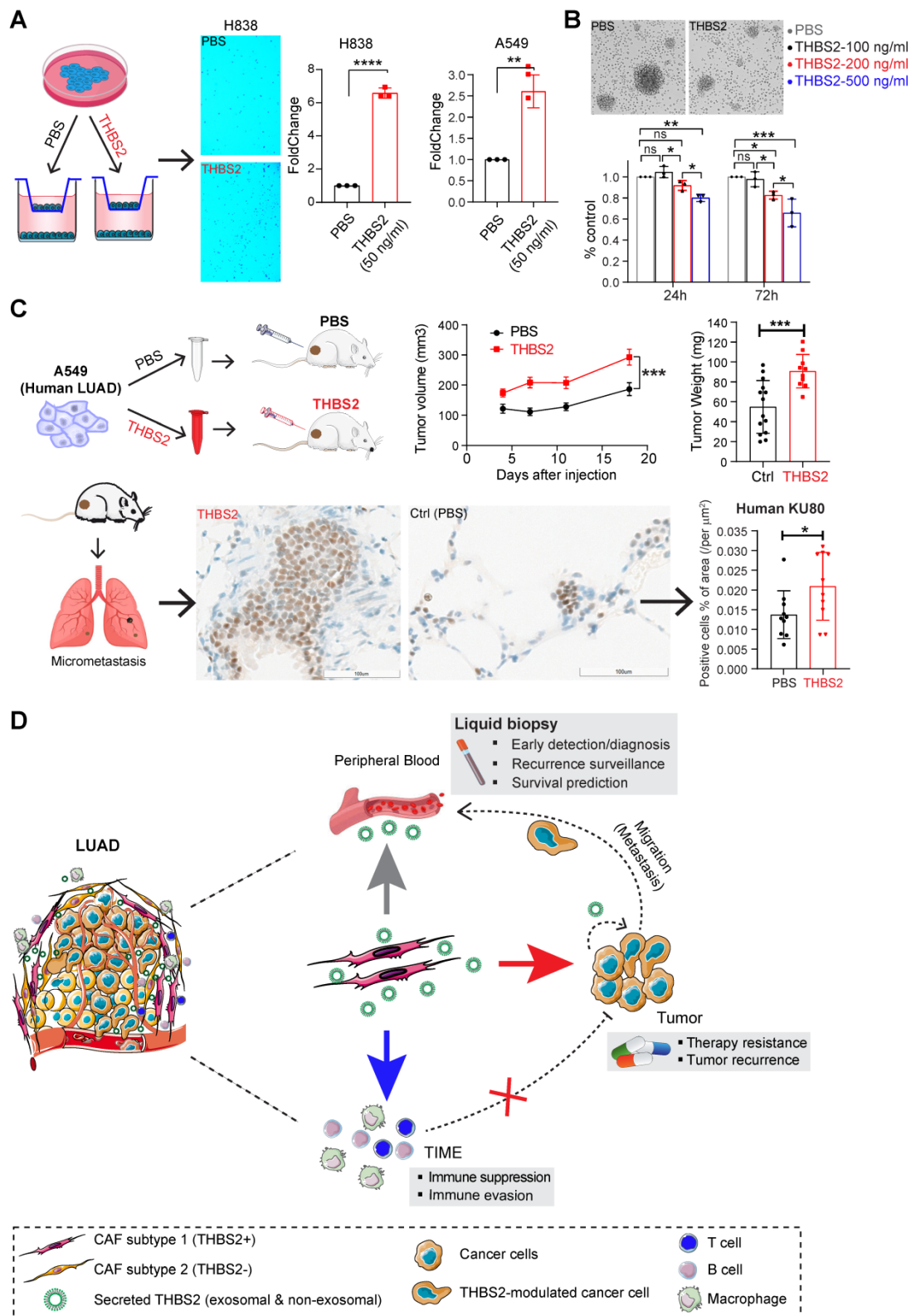


Figure 10. THBS2 plays a pleiotropic role in modulating cancer cells and immune cells. A, *In vitro* Transwell assays showing the effect of THBS2 on the migration of human A549 and H838 LUAD (lung adenocarcinoma) cells. Representative images (10x) of H838-Transwell assays were shown in the middle. **** $p < 0.0001$ by two-sided student's t-test. B, *Ex vivo* T cell proliferation assay showing the effect of THBS2 (96h) on the proliferation of activated CD3+ T cells. The representative image on the top is under the treatment 500 ng/mL THBS2 recombinant protein. C, *In vivo* LUAD xenografts showing the effect of THBS2 on subcutaneous tumor growth (upper panel) and micro-metastasis to the lung (lower panel), with the quantifications shown to the right. Human-specific KU80 antibody was used to detect human-derived A549 LUAD cells. To make the analysis comparable, the number of positive cells was normalized to the scanned area (per μm^2). *** $p < 0.001$ by two-way ANOVA test (tumor volume). ** $p < 0.01$; *** $p < 0.001$ by two-sided student's t-test. D, A hypothetical model illustrating the pleiotropic roles of THBS2 in the micro-ecosystem of LUAD. 1) Secreted THBS2 can be detected in peripheral blood, thus as a promising liquid biomarker; 2) THBS2 promotes tumor recurrence/metastasis/treatment resistance; 3) THBS2 promotes an immune-suppressive microenvironment by interacting with immune cells, thereby facilitating the immune escape of LUAD tumor cells. Figures were created with BioRender.com. TIME: tumor immune microenvironment. CAF: cancer-associated fibroblasts.

We further revealed the potential functions of THBS2+ CAFs, indicating that this subset possesses a potential capacity to modulate the cancer cells and, in particular, TME. Our findings were in line with previous evidence demonstrating that glycoproteins played a role in modulating immunity [78] and that subsets of CAFs are a major source of immunosuppressive activity in the TME [73, 74]. Concerning its implications for clinical immunotherapy, we observed a negative association of THBS2 expression with the response to immunotherapy. As such, strategies targeting THBS2+ CAFs might be a potential treatment strategy for this aggressive subset. Recent attempts to therapeutically target CAFs (specifically depleting α SMA+ CAFs) failed in preclinical models of pancreatic cancer and even potentially worsened patients' prognosis [88], which was, in part, due to an incomplete understanding of CAF heterogeneity. Targeting other populations of CAFs instead of α SMA+ in a specific context might provide benefits. Together, we provided the first evidence that targeting THBS2+ CAFs might have promises to improve the patients' prognosis and response to multiple therapeutics.

Beyond defining an aggressive subset of early-stage LUAD, we also observed that a high expression of THBS2 predicts poor prognosis in LUAD patients treated with clinical chemotherapy, EGFR-TKIs-targeted therapy or immunotherapy (**Figure S4B, S4E; Figure 9**), which warrants further validations with large clinical cohorts. Nevertheless, these observations suggest a potential role of THBS2+ CAFs in promoting treatment failure, which is in line with the increasingly essential role of CAFs in therapy resistance [74, 89]. Further, it remains to be defined whether THBS2 itself or other proteins/components secreted by THBS2+ CAFs contribute to that phenotype.

Our evidence has shown that THBS2 has been shuttled via exosomes (**Figure 4; Figure S6**) [87], and exosome-mediated intercellular communication predominantly occurs in three ways [90]: 1) exosome membrane protein can directly bind to the membrane protein of target cells, leading to activating the signaling pathway; 2) in the extracellular matrix, a protease can cleave the exosome membrane protein, and then bind to receptors on the cell membrane of target cells, consequently activating the downstream signaling pathway; 3) the exosome membrane can directly fuse with the cell membrane of target cells, releasing its contents (e.g., proteins, RNA or DNA) into the target cells. Our data indicated that exosomal THBS2 resides on the surface membrane rather than inside of the secreted exosomes, implying that it is likely to function through directly binding to the

membrane protein of its target cells, which is similar to that of non-exosomal THBS2. Also, the above three ways might occur simultaneously. As such, it remains to define whether the released contents contained in exosomes, e.g. DNA, RNA, or other proteins beyond THBS2, exert effects on the target cells. Specifically and selectively delivering THBS2 by means of engineering exosomes may provide valuable insights [91]. Collectively, our results indicate THBS2 is likely to function through exosomal and non-exosomal forms, and whether these two forms of THBS2 play different roles in promoting the progression of LUAD requires systematic investigations.

Of note, CD36 and CD47 are two well-characterized receptors of THBS2 [80]. Recent evidence demonstrated that CD36 was selectively upregulated in intratumoral Treg cells [81] and also promoted intratumoral CD8+ T cell dysfunction [82]. Thus, targeting CD36 could greatly enhance antitumor responses with anti-PD-1 therapy [81, 82]. CD47, a 'marker-of-self' protein that is broadly overexpressed across tumor cells, is also emerging as a novel macrophage immune checkpoint for cancer immunotherapy [83]. Interestingly, our mIHC data showed that THBS2 potentially predominantly affected B, CD8+ T cells and macrophages, and THBS2 expression was inversely associated with CD8+ T cell infiltrates (**Figure 7F-H; Figure 8; Figure S14**). Functionally, THBS2 suppressed the proliferation of CD3+ T cells infiltrates (**Figure 10B**), which in line with a previous study showing that the peptide 4N1K, conserved in all thrombospondin isoforms and mimics the activity of the COOH-terminal cell-binding domain, induces the death of activated, but not resting T cells, via a CD47-dependent mechanism [92]. Nevertheless, detailed mechanistic insights into how THBS2+ CAFs shape tumor immunity and modulate the immunotherapy response warrant further study. Intriguingly, recent evidence shows that TGF- β 1-THBS2 feedback circuit plays a key role in promoting the progression of pancreatic ductal adenocarcinoma (PDAC) [93]. Mechanistically, cancer cell-secreted TGF- β 1 activated CAFs to induce THBS2 expression through the Smad2/3 pathway. Then, CAF-derived THBS2 binds to its cognate receptors integrin α v β 3/CD36, leading to the activation of MAPK pathway to promote tumor growth.

Limitations

There are some limitations of this study. For instance, there is a lack of a large and independent LUAD cohort to validate exosomal THBS2 as an effective biomarker to define high-risk early-stage LUAD populations. Likewise, the sample size for the

multiplexed IHC investigating the association between THBS2 and immune cell infiltrates was very small, thus requiring an extended sample size for further validation. Furthermore, a direct validation with CAFs-derived THBS2 by culturing and purifying clinical LUAD samples is also needed. Also, we did not explore the role of exosomal THBS2 in the progress of LUAD, which requires systematic investigations in the future.

Conclusions

Overall, we uncovered a biomarker THBS2, produced by a subset of tumor-specific THBS2+ CAF subpopulation, to stratify a subgroup of early-stage LUAD patients. THBS2 might play a pleiotropic role in modulating cancer cells and particularly tumor immunity. Our study provides not only a biomarker for predicting clinical outcomes of pN0-stage LUAD but also a potential target for therapeutic intervention.

Abbreviations

CAF: cancer-associated fibroblast; ECM: extracellular matrix; EGFR-TKIs: epidermal growth factor receptor tyrosine kinase inhibitors; GSEA: gene set enrichment analysis; IHC: Immunohistochemistry; LUAD: lung adenocarcinoma; LUSC: lung squamous cell carcinoma; mIHC: Multiplexed IHC; NTA: nanoparticle tracking analysis; OS: overall survival; RFS: recurrence-free survival; scRNA-seq: single-cell RNA sequencing; TCGA: The Cancer Genome Atlas; TEM: transmission electron microscopy; TIME: tumor immune microenvironment; TME: tumor microenvironment; WGCNA: weighted gene co-expression analysis.

Supplementary Material

Supplementary figures.

<https://www.thno.org/v12p3104s1.pdf>

Acknowledgements

This study used the databases from TCGA Program and GEO, and the authors acknowledge the efforts of the corresponding institutes. The interpretation and reporting of these data are the sole responsibility of the authors.

Financial support

This research was supported by National Natural Science Foundation of China (82072570 to F.Y; 82002941 to B.S); Excellent talent program of Shanghai Chest Hospital (to F.Y); Clinical science and technology innovation project of Shanghai Hospital Development Center (SHDC12018113 to W.G).

Ethics approval and consent to participate

This study was approved by the institutional review board (#KS(Y)21316). All patients had signed informed consent for inclusion of their clinical data and specimens in our Lung Biobank and use in research projects, according to the recommendation of the ethical committee of Shanghai Chest Hospital. All the procedures were performed in accordance with the 1964 Declaration of Helsinki principles and its later amendments or comparable ethical standards. All animal experiments were carried out in accordance with the guidelines published by the Institutional Animal Care and Use Committee of Shanghai Chest Hospital, Shanghai Jiao Tong University.

Availability of data and materials

The authors declare that all the data supporting the findings in this study are available in this study and its Supplementary materials, or are available from the corresponding author through reasonable request. scRNA-seq data have been deposited in NCBI's Gene Expression Omnibus and are accessible through GEO Series accession number GSE198099.

Competing Interests

The authors have declared that no competing interest exists.

References

1. de Koning HJ, van der Aalst CM, de Jong PA, Scholten ET, Nackaerts K, Heuvelmans MA, et al. Reduced Lung-Cancer Mortality with Volume CT Screening in a Randomized Trial. *N Engl J Med.* 2020; 382: 503-13.
2. Zhang J, Wu J, Tan Q, Zhu L, Gao W. Why do pathological stage IA lung adenocarcinomas vary from prognosis?: a clinicopathologic study of 176 patients with pathological stage IA lung adenocarcinoma based on the IASLC/ATS/ERS classification. *J Thorac Oncol.* 2013; 8: 1196-202.
3. Yoshizawa A, Motoi N, Riely GJ, Sima CS, Gerald WL, Kris MG, et al. Impact of proposed IASLC/ATS/ERS classification of lung adenocarcinoma: prognostic subgroups and implications for further revision of staging based on analysis of 514 stage I cases. *Mod Pathol.* 2011; 24: 653-64.
4. Hung JJ, Yeh YC, Jeng WJ, Wu KJ, Huang BS, Wu YC, et al. Predictive value of the international association for the study of lung cancer/American Thoracic Society/European Respiratory Society classification of lung adenocarcinoma in tumor recurrence and patient survival. *J Clin Oncol.* 2014; 32: 2357-64.
5. Lopez Guerra JL, Gomez DR, Lin SH, Levy LB, Zhuang Y, Komaki R, et al. Risk factors for local and regional recurrence in patients with resected N0-N1 non-small-cell lung cancer, with implications for patient selection for adjuvant radiation therapy. *Ann Oncol.* 2013; 24: 67-74.
6. Wu CF, Fu JY, Yeh CJ, Liu YH, Hsieh MJ, Wu YC, et al. Recurrence Risk Factors Analysis for Stage I Non-small Cell Lung Cancer. *Medicine (Baltimore).* 2015; 94: e1337.
7. David E, Thall PF, Kalhor N, Hofstetter WL, Rice DC, Roth JA, et al. Visceral pleural invasion is not predictive of survival in patients with lung cancer and smaller tumor size. *Ann Thorac Surg.* 2013; 95: 1872-7; discussion 7.
8. Douillard JY, Rosell R, De Lena M, Carpagnano F, Ramlau R, Gonzales-Larriba JL, et al. Adjuvant vinorelbine plus cisplatin versus observation in patients with completely resected stage IB-IIIa non-small-cell lung cancer (Adjuvant Navelbine International Trialist Association [ANITA]): a randomised controlled trial. *Lancet Oncol.* 2006; 7: 719-27.
9. Qian J, Xu J, Wang S, Qian F, Yang W, Zhang B, et al. Adjuvant Chemotherapy Candidates in Stage I Lung Adenocarcinomas Following Complete Lobectomy. *Ann Surg Oncol.* 2019; 26: 2392-400.
10. Morgensztern D, Du L, Waqar SN, Patel A, Samson P, Devarakonda S, et al. Adjuvant Chemotherapy for Patients with T2N0M0 NSCLC. *J Thorac Oncol.* 2016; 11: 1729-35.
11. Strauss GM, Herndon JE, 2nd, Maddaus MA, Johnstone DW, Johnson EA, Harpole DH, et al. Adjuvant paclitaxel plus carboplatin compared with

- observation in stage IB non-small-cell lung cancer: CALGB 9633 with the Cancer and Leukemia Group B, Radiation Therapy Oncology Group, and North Central Cancer Treatment Group Study Groups. *J Clin Oncol.* 2008; 26: 5043-51.
12. Corcoran RB. Liquid biopsy versus tumor biopsy for clinical-trial recruitment. *Nat Med.* 2020; 26: 1815-6.
 13. Yu W, Hurley J, Roberts D, Chakraborty SK, Enderle D, Noerholm M, et al. Exosome-based liquid biopsies in cancer: opportunities and challenges. *Ann Oncol.* 2021; 32: 466-77.
 14. Azmi AS, Bao B, Sarkar FH. Exosomes in cancer development, metastasis, and drug resistance: a comprehensive review. *Cancer Metastasis Rev.* 2013; 32: 623-42.
 15. Bejarano L, Jordao MJC, Joyce JA. Therapeutic Targeting of the Tumor Microenvironment. *Cancer Discov.* 2021; 11: 933-59.
 16. Biffi G, Tuveson DA. Diversity and Biology of Cancer-Associated Fibroblasts. *Physiol Rev.* 2021; 101: 147-76.
 17. Hu JL, Wang W, Lan XL, Zeng ZC, Liang YS, Yan YR, et al. CAFs secreted exosomes promote metastasis and chemotherapy resistance by enhancing cell stemness and epithelial-mesenchymal transition in colorectal cancer. *Mol Cancer.* 2019; 18: 91.
 18. Langfelder P, Horvath S. WGCNA: an R package for weighted correlation network analysis. *BMC Bioinformatics.* 2008; 9: 559.
 19. Yang H, Xu D, Yang Z, Yao F, Zhao H, Schmid RA, et al. Systematic Analysis of Aberrant Biochemical Networks and Potential Drug Vulnerabilities Induced by Tumor Suppressor Loss in Malignant Pleural Mesothelioma. *Cancers (Basel).* 2020; 12.
 20. Zhang T, Yang H, Sun B, Yao F. Four hub genes regulate tumor infiltration by immune cells, antitumor immunity in the tumor microenvironment, and survival outcomes in lung squamous cell carcinoma patients. *Aging (Albany NY).* 2021; 12.
 21. Yu G, Wang LG, Han Y, He QY. clusterProfiler: an R package for comparing biological themes among gene clusters. *OMICS.* 2012; 16: 284-7.
 22. Yang H, Zhao L, Gao Y, Yao F, Marti TM, Schmid RA, et al. Pharmacotranscriptomic Analysis Reveals Novel Drugs and Gene Networks Regulating Ferroptosis in Cancer. *Cancers (Basel).* 2020; 12: 3273.
 23. Schwartz LH, Litiere S, de Vries E, Ford R, Gwyther S, Mandrekar S, et al. RECIST 1.1-Update and clarification: From the RECIST committee. *Eur J Cancer.* 2016; 62: 132-7.
 24. Butler A, Hoffman P, Smibert P, Papalexi E, Satija R. Integrating single-cell transcriptomic data across different conditions, technologies, and species. *Nature biotechnology.* 2018; 36: 411-20.
 25. Wolock SL, Lopez R, Klein AM. Scrublet: Computational Identification of Cell Doublets in Single-Cell Transcriptomic Data. *Cell Syst.* 2019; 8: 281-91 e9.
 26. Stuart T, Butler A, Hoffman P, Hafemeister C, Papalexi E, Mauck WM, 3rd, et al. Comprehensive Integration of Single-Cell Data. *Cell.* 2019; 177: 1888-902 e21.
 27. Zappia L, Oshlack A. Clustering trees: a visualization for evaluating clusterings at multiple resolutions. *Gigascience.* 2018; 7.
 28. Wu T, Hu E, Xu S, Chen M, Guo P, Dai Z, et al. clusterProfiler 4.0: A universal enrichment tool for interpreting omics data. *Innovation (NY).* 2021; 2: 100141.
 29. Subramanian A, Tamayo P, Mootha VK, Mukherjee S, Ebert BL, Gillette MA, et al. Gene set enrichment analysis: a knowledge-based approach for interpreting genome-wide expression profiles. *Proceedings of the National Academy of Sciences of the United States of America.* 2005; 102: 15545-50.
 30. Jin S, Guerrero-Juarez CF, Zhang L, Chang J, Ramos R, Kuan CH, et al. Inference and analysis of cell-cell communication using CellChat. *Nature communications.* 2021; 12: 1088.
 31. Wei R, Zhao L, Kong G, Liu X, Zhu S, Zhang S, et al. Combination of Size-Exclusion Chromatography and Ultracentrifugation Improves the Proteomic Profiling of Plasma-Derived Small Extracellular Vesicles. *Biol Proced Online.* 2020; 22: 12.
 32. Vella LJ, Scicluna BJ, Cheng L, Bowden EG, Masters CL, Ang CS, et al. A rigorous method to enrich for exosomes from brain tissue. *J Extracell Vesicles.* 2017; 6: 1348885.
 33. Crescitelli R, Lasser C, Lotvall J. Isolation and characterization of extracellular vesicle subpopulations from tissues. *Nat Protoc.* 2021; 16: 1548-80.
 34. Torres VI, Barrera DP, Varas-Godoy M, Arancibia D, Inestrosa NC. Selective Surface and Intraluminal Localization of Wnt Ligands on Small Extracellular Vesicles Released by HT-22 Hippocampal Neurons. *Front Cell Dev Biol.* 2021; 9: 735888.
 35. Yang H, Liang SQ, Xu D, Yang Z, Marti TM, Gao Y, et al. HSP90/AXL/eIF4E-regulated unfolded protein response as an acquired vulnerability in drug-resistant KRAS-mutant lung cancer. *Oncogenesis.* 2019; 8: 45.
 36. Neachou IP, Lillard K, Gavriel CG, Ueno H, Harrison DJ, Caie PD. Automated Analysis of Lymphocytic Infiltration, Tumor Budding, and Their Spatial Relationship Improves Prognostic Accuracy in Colorectal Cancer. *Cancer Immunol Res.* 2019; 7: 609-20.
 37. Fedor HL, De Marzo AM. Practical methods for tissue microarray construction. *Methods Mol Med.* 2005; 103: 89-101.
 38. Bankhead P, Loughrey MB, Fernandez JA, Dombrowski Y, McArt DG, Dunne PD, et al. QuPath: Open source software for digital pathology image analysis. *Sci Rep.* 2017; 7: 16878.
 39. Landi MT, Dracheva T, Rotunno M, Figueroa JD, Liu H, Dasgupta A, et al. Gene expression signature of cigarette smoking and its role in lung adenocarcinoma development and survival. *PLoS One.* 2008; 3: e1651.
 40. Selamat SA, Chung BS, Girard L, Zhang W, Zhang Y, Campan M, et al. Genome-scale analysis of DNA methylation in lung adenocarcinoma and integration with mRNA expression. *Genome Res.* 2012; 22: 1197-211.
 41. Robles AI, Arai E, Mathe EA, Okayama H, Schetter AJ, Brown D, et al. An Integrated Prognostic Classifier for Stage I Lung Adenocarcinoma Based on mRNA, microRNA, and DNA Methylation Biomarkers. *J Thorac Oncol.* 2015; 10: 1037-48.
 42. Beer DG, Kardina SL, Huang CC, Giordano TJ, Levin AM, Misek DE, et al. Gene-expression profiles predict survival of patients with lung adenocarcinoma. *Nat Med.* 2002; 8: 816-24.
 43. Schabath MB, Welsh EA, Fulp WJ, Chen L, Teer JK, Thompson ZJ, et al. Differential association of STK11 and TP53 with KRAS mutation-associated gene expression, proliferation and immune surveillance in lung adenocarcinoma. *Oncogene.* 2016; 35: 3209-16.
 44. Rousseaux S, Debernardi A, Jacquiau B, Vitte AL, Vesin A, Nagy-Mignotte H, et al. Ectopic activation of germline and placental genes identifies aggressive metastasis-prone lung cancers. *Sci Transl Med.* 2013; 5: 186a66.
 45. Xie Y, Xiao G, Coombes KR, Behrens C, Solis LM, Raso G, et al. Robust gene expression signature from formalin-fixed paraffin-embedded samples predicts prognosis of non-small-cell lung cancer patients. *Clin Cancer Res.* 2011; 17: 5705-14.
 46. Zhu CQ, Ding K, Strumpf D, Weir BA, Meyerson M, Pennell N, et al. Prognostic and predictive gene signature for adjuvant chemotherapy in resected non-small-cell lung cancer. *J Clin Oncol.* 2010; 28: 4417-24.
 47. Zhang L, Li M, Deng B, Dai N, Feng Y, Shan J, et al. HLA-DQB1 expression on tumor cells is a novel favorable prognostic factor for relapse in early-stage lung adenocarcinoma. *Cancer Manag Res.* 2019; 11: 2605-16.
 48. Chen J, Yang H, Teo ASM, Amer LB, Sherbaf FG, Tan CQ, et al. Genomic landscape of lung adenocarcinoma in East Asians. *Nat Genet.* 2020; 52: 177-86.
 49. Chen YJ, Roumeliotis TI, Chang YH, Chen CT, Han CL, Lin MH, et al. Proteogenomics of Non-smoking Lung Cancer in East Asia Delineates Molecular Signatures of Pathogenesis and Progression. *Cell.* 2020; 182: 226-44 e17.
 50. Gillette MA, Satpathy S, Cao S, Dhanasekaran SM, Vasaikar SV, Krug K, et al. Proteogenomic Characterization Reveals Therapeutic Vulnerabilities in Lung Adenocarcinoma. *Cell.* 2020; 182: 200-25 e35.
 51. Xu JY, Zhang C, Wang X, Zhai L, Ma Y, Mao Y, et al. Integrative Proteomic Characterization of Human Lung Adenocarcinoma. *Cell.* 2020; 182: 245-61 e17.
 52. Lanczky A, Gyorffy B. Web-Based Survival Analysis Tool Tailored for Medical Research (KMPlot): Development and Implementation. *J Med Internet Res.* 2021; 23: e27633.
 53. Shi R, Bao X, Unger K, Sun J, Lu S, Manapov F, et al. Identification and validation of hypoxia-derived gene signatures to predict clinical outcomes and therapeutic responses in stage I lung adenocarcinoma patients. *Theranostics.* 2021; 11: 5061-76.
 54. Li J, Lu Y, Akbani R, Ju Z, Roebuck PL, Liu W, et al. TCPA: a resource for cancer functional proteomics data. *Nat Methods.* 2013; 10: 1046-7.
 55. Jung H, Kim HS, Kim JY, Sun JM, Ahn JS, Ahn MJ, et al. DNA methylation loss promotes immune evasion of tumours with high mutation and copy number load. *Nat Commun.* 2019; 10: 4278.
 56. Hugo W, Zaretsky JM, Sun L, Song C, Moreno BH, Hu-Lieskovan S, et al. Genomic and Transcriptomic Features of Response to Anti-PD-1 Therapy in Metastatic Melanoma. *Cell.* 2016; 165: 35-44.
 57. Lesterhuis WJ, Rinaldi C, Jones A, Rozali EN, Dick IM, Khong A, et al. Network analysis of immunotherapy-induced regressing tumours identifies novel synergistic drug combinations. *Sci Rep.* 2015; 5: 12298.
 58. Thorsson V, Gibbs DL, Brown SD, Wolf D, Bortone DS, Ou Yang TH, et al. The Immune Landscape of Cancer. *Immunity.* 2018; 48: 812-30 e14.
 59. Bagaev A, Kotlov N, Nomie K, Svekolkin V, Gafurov A, Isaeva O, et al. Conserved pan-cancer microenvironment subtypes predict response to immunotherapy. *Cancer Cell.* 2021; 39: 845-65 e7.
 60. Finotello F, Mayer C, Plattner C, Laschober G, Rieder D, Hackl H, et al. Molecular and pharmacological modulators of the tumor immune contexture revealed by deconvolution of RNA-seq data. *Genome Med.* 2019; 11: 34.
 61. Yang H, Berezowska S, Dorn P, Zens P, Chen P, Peng RW, et al. Tumor-infiltrating lymphocytes are functionally inactivated by CD90+ stromal cells and reactivated by combined Ibrutinib and Rapamycin in human pleural mesothelioma. *Theranostics.* 2022; 12: 167-85.
 62. Wang L, Yang H, Dorn P, Berezowska S, Blank F, Wotzkow C, et al. Peritumoral CD90+CD73+ cells possess immunosuppressive features in human non-small cell lung cancer. *EBioMedicine.* 2021; 73: 103664.
 63. Yang H, Sun B, Xu K, He Y, Zhang T, Hall SRR, et al. Pharmacotranscriptomic correlation analysis reveals novel responsive signatures to HDAC inhibitors and identifies Dasatinib as a synergistic interactor in small-cell lung cancer. *EBioMedicine.* 2021; 69: 103457.
 64. Jiang YM, Yu DL, Hou GX, Jiang JL, Zhou Q, Xu XF. Serum thrombospondin-2 is a candidate diagnosis biomarker for early non-small-cell lung cancer. *Biosci Rep.* 2019; 39.
 65. Ettrich TJ, Berger AW, Schwerdel D, Reinacher-Schick AC, Uhl W, Alguet H, et al. A blood-based assay for diagnosis of early-stage pancreatic cancer. *Journal of Clinical Oncology.* 2019; 37: 234-.

66. Kim J, Bamlet WR, Oberg AL, Chaffee KG, Donahue G, Cao XJ, et al. Detection of early pancreatic ductal adenocarcinoma with thrombospondin-2 and CA19-9 blood markers. *Sci Transl Med.* 2017; 9.
67. Sun R, Wu J, Chen Y, Lu M, Zhang S, Lu D, et al. Down regulation of Thrombospondin2 predicts poor prognosis in patients with gastric cancer. *Mol Cancer.* 2014; 13: 225.
68. Dvorkina M, Nieddu V, Chakelam S, Pezzolo A, Cantilena S, Leite AP, et al. A Promyelocytic Leukemia Protein-Thrombospondin-2 Axis and the Risk of Relapse in Neuroblastoma. *Clin Cancer Res.* 2016; 22: 3398-409.
69. Weng TY, Wang CY, Hung YH, Chen WC, Chen YL, Lai MD. Differential Expression Pattern of THBS1 and THBS2 in Lung Cancer: Clinical Outcome and a Systematic-Analysis of Microarray Databases. *PLoS One.* 2016; 11: e0161007.
70. Costa AF, Campos D, Reis CA, Gomes C. Targeting Glycosylation: A New Road for Cancer Drug Discovery. *Trends Cancer.* 2020; 6: 757-66.
71. Wu YL, Tsuboi M, He J, John T, Grohe C, Majem M, et al. Osimertinib in Resected EGFR-Mutated Non-Small-Cell Lung Cancer. *N Engl J Med.* 2020; 383: 1711-23.
72. Roper N, Brown AL, Wei JS, Pack S, Trindade C, Kim C, et al. Clonal Evolution and Heterogeneity of Osimertinib Acquired Resistance Mechanisms in EGFR Mutant Lung Cancer. *Cell Rep Med.* 2020; 1.
73. Costa A, Kieffer Y, Scholer-Dahirel A, Pelon F, Bourachot B, Cardon M, et al. Fibroblast Heterogeneity and Immunosuppressive Environment in Human Breast Cancer. *Cancer Cell.* 2018; 33: 463-79 e10.
74. Hu H, Piotrowska Z, Hare PJ, Chen H, Mulvey HE, Mayfield A, et al. Three subtypes of lung cancer fibroblasts define distinct therapeutic paradigms. *Cancer Cell.* 2021; 39: 1531-47 e10.
75. Lambrechts D, Wauters E, Boeckx B, Aibar S, Nittner D, Burton O, et al. Phenotype molding of stromal cells in the lung tumor microenvironment. *Nat Med.* 2018; 24: 1277-89.
76. Sun D, Wang J, Han Y, Dong X, Ge J, Zheng R, et al. TISCH: a comprehensive web resource enabling interactive single-cell transcriptome visualization of tumor microenvironment. *Nucleic Acids Res.* 2021; 49: D1420-D30.
77. Chakravarthy A, Khan L, Bensler NP, Bose P, De Carvalho DD. TGF-beta-associated extracellular matrix genes link cancer-associated fibroblasts to immune evasion and immunotherapy failure. *Nat Commun.* 2018; 9: 4692.
78. Baghdadi M, Yoneda A, Yamashina T, Nagao H, Komohara Y, Nagai S, et al. TIM-4 glycoprotein-mediated degradation of dying tumor cells by autophagy leads to reduced antigen presentation and increased immune tolerance. *Immunity.* 2013; 39: 1070-81.
79. Chen L, Cao MF, Zhang X, Dang WQ, Xiao JF, Liu Q, et al. The landscape of immune microenvironment in lung adenocarcinoma and squamous cell carcinoma based on PD-L1 expression and tumor-infiltrating lymphocytes. *Cancer Med.* 2019; 8: 7207-18.
80. Lawler PR, Lawler J. Molecular basis for the regulation of angiogenesis by thrombospondin-1 and -2. *Cold Spring Harb Perspect Med.* 2012; 2: a006627.
81. Wang H, Franco F, Tsui YC, Xie X, Trefny MP, Zappasodi R, et al. CD36-mediated metabolic adaptation supports regulatory T cell survival and function in tumors. *Nat Immunol.* 2020; 21: 298-308.
82. Xu S, Chaudhary O, Rodriguez-Morales P, Sun X, Chen D, Zappasodi R, et al. Uptake of oxidized lipids by the scavenger receptor CD36 promotes lipid peroxidation and dysfunction in CD8(+) T cells in tumors. *Immunity.* 2021; 54: 1561-77 e7.
83. Feng R, Zhao H, Xu J, Shen C. CD47: the next checkpoint target for cancer immunotherapy. *Crit Rev Oncol Hematol.* 2020; 152: 103014.
84. Rakaee M, Busund LR, Jamaly S, Paulsen EE, Richardsen E, Andersen S, et al. Prognostic Value of Macrophage Phenotypes in Resectable Non-Small Cell Lung Cancer Assessed by Multiplex Immunohistochemistry. *Neoplasia.* 2019; 21: 282-93.
85. Carrega P, Morandi B, Costa R, Frumento G, Forte G, Altavilla G, et al. Natural killer cells infiltrating human nonsmall-cell lung cancer are enriched in CD56 bright CD16(-) cells and display an impaired capability to kill tumor cells. *Cancer.* 2008; 112: 863-75.
86. Goldstraw P, Chansky K, Crowley J, Rami-Porta R, Asamura H, Eberhardt WE, et al. The IASLC Lung Cancer Staging Project: Proposals for Revision of the TNM Stage Groupings in the Forthcoming (Eighth) Edition of the TNM Classification for Lung Cancer. *J Thorac Oncol.* 2016; 11: 39-51.
87. Hoshino A, Kim HS, Bojmar L, Gyan KE, Cioffi M, Hernandez J, et al. Extracellular Vesicle and Particle Biomarkers Define Multiple Human Cancers. *Cell.* 2020; 182: 1044-61 e18.
88. Ozdemir BC, Pentcheva-Hoang T, Carstens JL, Zheng X, Wu CC, Simpson TR, et al. Depletion of carcinoma-associated fibroblasts and fibrosis induces immunosuppression and accelerates pancreas cancer with reduced survival. *Cancer Cell.* 2014; 25: 719-34.
89. Domen A, Quatannens D, Zanivan S, Deben C, Van Audenaerde J, Smits E, et al. Cancer-Associated Fibroblasts as a Common Orchestrator of Therapy Resistance in Lung and Pancreatic Cancer. *Cancers (Basel).* 2021; 13.
90. Guo Y, Ji X, Liu J, Fan D, Zhou Q, Chen C, et al. Effects of exosomes on pre-metastatic niche formation in tumors. *Mol Cancer.* 2019; 18: 39.
91. Liang Y, Duan L, Lu J, Xia J. Engineering exosomes for targeted drug delivery. *Theranostics.* 2021; 11: 3183-95.
92. Lamy L, Foussat A, Brown EJ, Bornstein P, Ticchioni M, Bernard A. Interactions between CD47 and thrombospondin reduce inflammation. *J Immunol.* 2007; 178: 5930-9.
93. Nan P, Dong X, Bai X, Lu H, Liu F, Sun Y, et al. Tumor-stroma TGF-beta1-THBS2 feedback circuit drives pancreatic ductal adenocarcinoma progression via integrin alphavbeta3/CD36-mediated activation of the MAPK pathway. *Cancer Lett.* 2022; 528: 59-75.